

A Thesis

entitled

Behavior of RC Beams Strengthened in Flexure by CFRP EBRIG

Technique

by

Milan Shrestha

Submitted to the Graduate Faculty as partial fulfillment of the requirements for the

Master of Science Degree in

Civil Engineering

Dr. Azadeh Parvin, Committee Chair

Dr. Liangbo Hu, Committee Member

Dr. Luis Alexander Mata, Committee Member

Dr. Scott Molitor, Acting Dean
College of Graduate Studies

The University of Toledo

August 2022

© 2022 Milan Shrestha

This document is copyrighted material. Under copyright law, no parts of this document may be reproduced without the expressed permission of the author.

An Abstract
of
Behavior of RC Beams Strengthened in Flexure by CFRP EBRIG Technique

by
Milan Shrestha

Submitted to the Graduate Faculty as partial fulfillment of the requirements for the
Master of Science Degree in
Civil Engineering

The University of Toledo
August 2022

The present study investigates the flexural strengthening by externally bonded reinforcement in groove (EBRIG) of reinforced concrete (RC) beams using various layers of carbon fiber reinforced polymers (CFRP). ANSYS Mechanical APDL software was used to model the beams which were validated through an existing experimental study in the literature. A parametric study was carried out on the validated finite element beam models. The parameters considered were the depth and number of grooves in EBRIG strengthened beams. Additionally, the beams were strengthened by combining EBRIG and near-surface mounting (NSM) technique, for which NSM FRP bar size was also investigated. For all strengthened beams, the load capacity improved with the increase in the number and depth of grooves. Furthermore, for the beams strengthened by the combined EBRIG-NSM technique with a single layer of CFRP, the ultimate load capacity enhanced with increased NSM FRP rod size. The maximum load capacity improvement achieved in EBRIG strengthened beam was 182.2% relative to the control beam when a triple layer of FRP and five grooves were provided. Increasing the number of grooves or

the size of NSM rods shifted the failure from FRP rupture to concrete spalling in beams strengthened with combined EBRIG-NSM techniques. The number and depth of grooves did not alter the failure mode of EBRIG strengthened beams.

Dedicated to my friends and family.

Acknowledgments

To begin with, I would like to express my sincere gratitude to my advisor and mentor, Dr. Azadeh Parvin, for providing me with proper guidance, helpful suggestions, and supervision. Her constant motivation expertise and constant support and motivation has been instrumental in the completion of this thesis.

Likewise, I am thankful to my master's thesis advisory committee: Dr. Liangbo Hu and Dr. Luis Alexander Mata for their valuable time and contributions throughout this process. In addition, I would like to acknowledge the faculty of the Department of Civil and Environmental Engineering for providing me an opportunity to pursue my Master's degree at the University of Toledo.

I express my sincere appreciation to my mother, father, and brother for their love and extraordinary support, which kept me motivated during the journey. At last, I would like to take this opportunity to thank my friends -Abhishek, Mukesh, Dwaypayan, Sujan, Rabin, Suba, Manoj, Upendra, who were always there to support me during my graduate life.

Table of Contents

Abstract.....	iii
Acknowledgments.....	vi
Table of Contents.....	vii
List of Tables.....	x
List of Figures	xi
List of Abbreviations.....	xiv
1. Introduction	1
1.1 Literature review.....	2
1.2 Methodology.....	14
1.3 Chapter 2 Summary	15
1.4 Chapter 3 Summary	15
1.5 Chapter 4 Summary	15
1.6 Chapter 5 Summary	15
1.7 Chapter 6 Summary	16
1.8 Chapter 7 Summary	16
2. Experimental Study for the Validation of FEA Beam Models.....	17
3. Finite Element Analysis Approach.....	20

3.1	Element Types	22
3.1.1	Concrete.....	22
3.1.2	Steel and FRP bars.....	23
3.1.3	FRP Sheets.....	24
3.1.4	Steel Plates and Epoxy Materials	25
3.1.5	Element Interfaces	26
3.2	Material Models.....	28
3.2.1	Concrete.....	28
3.2.2	Steel	31
3.2.2	CFRP	32
3.2.3	Epoxy Materials.....	33
3.2.4	Cohesive Zone Materials	34
3.3.	Boundary Conditions	36
3.4.	Nonlinear Analysis and Failure Modes	38
4.	Validation of FEA Beam Models	39
5.	Parametric Study.....	42
5.1	Effect of Groove Depth on EBRIG Strengthened RC Beams with Various Number of CFRP layers.....	43
5.2	Effect of Number of Grooves on EBRIG Strengthened RC Beams with Various Number of CFRP layers.....	47
5.3	Combined EBRIG and NSM Strengthening of RC Beams	51

5.4	Effect of Different Groove Depths on Combined EBRIG-NSM Rod Strengthened Beams.....	55
5.5	Effect of Various Number of Grooves on Combined EBRIG-NSM Rod Strengthened Beams.....	59
6.	Conclusions	63
7.	Recommendations and Future Work	66
7.1	Recommendations	66
7.2	Future work.....	66
Appendix A.....		75
	ANSYS APDL Code of RC Control Beam (CB).....	75
	ANSYS APDL Code of EBRIG Strengthened RC beam with single layer of CFRP (S2)	89

List of Tables

1.1 Studies on EBRIG strengthening technique.	12
4.1 Comparison of experiment and FEM results	39
5.1 Ultimate load capacity of beams strengthened by different layers of EBRIG with varying groove depth44	
5.2 Ultimate Load Capacity of Beams Strengthened by Various Layers of EBRIG and Groove Numbers.....	48
5.3 Ultimate Load Capacity of Beams Strengthened by Combined EBRIG-NSM Rods. 52	
5.4 Ultimate Load Capacity of Combined EBRIG-NSM Rods Strengthened Beams with Various Groove Depth.....	56
5.5 Ultimate Load Capacity of Combined EBRIG-NSM Rods Strengthened Beams with Various Groove Numbers	59

List of Figures

1.1 CFRP Fabric	5
1.2 CFRP Plates	6
1.3 CFRP rods	7
1.4 EBR strengthening technique (ACI440.2R, 2017).	8
1.5 NSM strengthening technique (ACI440.2R, 2017).	9
1.6 EBROG strengthening technique (Mostofinejad & Shameli, 2013)	10
1.7 EBRIG strengthening technique (Mostofinejad & Shameli, 2013)	11
2.1 Schematic view of the beam: (a) side view, (b) 3-D view, (c) size and spacing of grooves (d) cross-section view of CB, (e) cross-section view of S1, S2 and S3. (all dimensions are in mm).....	19
3.1 FE Models of Beam (a) 3D view, (b) Cross-section view, (c) Cross-section view, and (d) CFRP sheets in FEA models	21
3.2 Solid65 (ANSYS, 2020).	22
3.3 Rebar modelling approaches: (a) smeared approach, (b) embedded approach, and (c) Discrete Approach (Chong, 2004).	23
3.4 LINK180 (ANSYS, 2020).	24
3.5 Steel reinforcement bar elements in FEA beam model.	24
3.6 SHELL181 (ANSYS, 2020).	25
3.7 SOLID185 (ANSYS, 2020).	26
3.8 TARGET170 (ANSYS, 2020).	27

3.9	CONTA174(ANSYS, 2020).....	27
3.10	Stress versus strain curve of concrete under compression.....	29
3.11	Stress-strain curve of concrete under tension.	30
3.12	Stress versus strain curve of steel reinforcement bars.	31
3.13	Composition of CFRP composites (Kaw, 2006).....	32
3.14	Stress versus strain curve of CFRP in the direction of fiber.....	33
3.15	Stress versus strain curve of epoxy material.....	33
3.16	Supports and loadings in FEA models.....	37
3.17	Symmetry boundary condition.....	37
4.1	Load versus displacement curves of experimental and FEA of (a) CB beam, (b)S1 beam, (c) S2 beam, and (d)S3 beam.	41
5.1	Cross-section view of strengthened beams: (a) EBRIG, (b) Combined EBRIG-NSM rods.	43
5.2	Load versus displacement curve of EBRIG strengthened beams with different groove depths for (a) single CFRP layer, (b) double CFRP layer, and (c) triple CFRP layer.	47
5.3	Load versus displacement curve of CBRIG strengthened beams with various groove numbers for (a) single CFRP layer, (b) double CFRP layer, and (c) triple CFRP layer.	50
5.4	Load versus displacement curve of beams strengthened by combined EBRIG-NSM rods with various rod diameters and (a) single CFRP layer, (b) double CFRP layer, and (c) triple CFRP layer.	55

5.5 Load versus displacement curve of beams strengthened by combined EBRIG-NSM rods with single layer of FRP and various groove depths with (a) 2 mm NSM rod, (b) 3 mm NSM rod, and (c) 4 mm NSM rod. 58

5.6 Load versus displacement curve of combined EBRIG-NSM rod strengthened beams with single layer of FRP and various number of grooves with (a) 2 mm NSM rods, (b) 3 mm NSM rods, and (c) 4 mm NSM rods. 62

List of Abbreviations

CFRP.....Carbon Fiber Reinforced Polymer

EBR.....Externally Bonded Reinforcement

EBRIG.....Externally Bonded Reinforcing in Grooves

EBROG.....Externally Bonded Reinforcing on Grooves

NSM.....Near-Surface Mounting

Chapter 1

Introduction

Retrofitting and strengthening of existing RC structures are necessary to address additional load capacity requirements due to changes in occupancy, updates in codes, design and construction errors, and structural deterioration by age and environmental exposure. Fiber Reinforced Polymers (FRPs) are one of the most popular materials for strengthening the structures because of several advantages like resistance to corrosion, durability in extreme exposure, admirable strength to weight ratio, easy application, low thermal conductivity, no size limitation, and least changes in shape and size of the original structure (Oehlers, 2006; Tamuzs et al., 2007; Duthinh & Starnes, 2004). FRPs can be used to strengthen the RC structures in flexure, shear, torsion, and compression.

Externally bonded reinforcement (EBR) and near-surface mounted (NSM) are common methods of FRP strengthening of RC structures. In the EBR method, FRP sheets are attached to the external sides or faces of concrete using epoxy adhesives. The major issue associated with EBR FRP strengthening is premature interface debonding, which prevents full utilization of the tensile capacity of FRP materials (Sharif et al., 1994; Malek et al., 1998; Nguyen et al., 2001). In NSM strengthening technique, FRP strips or rods are installed in the grooves made on the concrete cover and are filled up with epoxy adhesives. Research shows that NSM FRP strengthening performs better in terms of load capacity

enhancement, and FRP material utilization. However, debonding is still an issue of NSM strengthening.

Externally bonded reinforcement in grooves (EBRIG) is a new FRP strengthening technique introduced by Mostofinejad and Shameli (Mostofinejad & Shameli, 2013). In EBRIG strengthening technique, grooves are cut on the concrete covers, FRP sheets are bonded on the internal surface of grooves as well as on the outside surface of the tension face of the beams, and the grooves are filled with epoxy materials. Very few studies are conducted on the FRP EBRIG strengthening of concrete beams in flexure and shear (Mostofinejad & Shameli, 2013; Mostofinejad et al., 2014; Shomali et al., 2019, 2020,2021). Studies have reported more load capacity enhancement by EBRIG strengthening technique than by EBR technique. Also, the premature debonding of FRP was either eliminated or delayed in case of EBRIG strengthening (Mostofinejad & Shameli, 2013; Mostofinejad et al., 2014; Shomali et al., 2021).

The following section presents the summary of studies on strengthening and retrofitting of concrete structures by the application of FRPs, needs for the further study of EBRIG strengthening technique.

1.1 Literature review

The FRP composites are the polymer matrix reinforced by fibers. The matrix can be either a thermosetting polymer such as polyester, vinyl ester, and epoxy or thermoplastic like nylon and polyethylene terephthalate. The most commonly used fibers in structural strengthening applications are glass, carbon, aramid, and basalt (ACI.2R, 2017; Bisby & Fitzwilliam, 2006; Jeevanantham et al., 2016; Kaw, 2005).

Glass Fibers

Glass fibers are the most commonly used fibers in structural application because of their low cost in comparison to other fibers. Glass fibers have high strength, moderate density and modulus of elasticity, and low thermal conductivity. Glass fibers are suitable for the structures which are not affected by increased weight and large deflections.

Carbon Fibers

Carbon fibers are characterized by high elasticity and strength, low weight, and thermal and chemical resistance. Carbon fibers are suitable for structures sensitive to weight and large deflection. Although carbon fibers are more expensive than glass fibers, structural applications of CFRP are increasing for the repair and retrofitting of concrete elements.

Aramid Fibers

Aramid fibers have high strength, moderate elasticity, and low weight. Aramid fibers are susceptible to radiation and moisture.

Basalt fibers

Basalt fibers have lower strength (about 50%) and stiffness (about 30%) relative to carbon fibers, but has higher ductility (about 200%). Also, basalt fabrics possess high resistance to heat and alkali, and excellent insulation properties.

The experimental study on FRP strengthening of concrete elements was reported around 1989 in Germany. Research in Switzerland paved the way for the first flexural strengthening application of externally bonded FRP on reinforced concrete bridges (Meier,

1987). First applications of the FRP system on RC columns were reported in Japan in the 1980s (Fardis & Khalil, 1981; Katsumata et al., 1987). Structural application of the FRP system escalated in Japan after the Hyogoken-Nanbu earthquake in 1995 (Nanni & Bradford, 1995}. Studies are being conducted on FRP reinforcement on concrete from the 1930s (ACI 440.2R, 2017). Retrofitting application of these system on concrete structures in US was started by National Science Foundation (NSF) and the Federal Highway Administration (FHWA) in the 1980s (ACI 440.2R, 2017). In present time, several codes and standards are available for the application of FRP systems for retrofitting of RC structures (ACI440.2R, 2017; JSCE, 2001; Model Code, 2010).

FRP composites are gaining more popularity from recent decades because of several advantages over conventional reinforcing steel strengthening of concrete structures. Some of them are (Singh, 2015):

- a. They have high longitudinal tensile strength.
- b. They are resistant to corrosion.
- c. They are unaffected by a magnetic field.
- d. They have high fatigue endurance.
- e. They are very light in weight. They have high strength to weight and stiffness to weight ratio.
- f. They have low thermal and electric conductivity.
- g. The installation process is easy and simple.

Despite having several advantages, FRP materials also have some disadvantages which call for attention when used as a structural strengthening material (Singh, 2015):

- a. The costs of these materials are relatively high.
- b. They are at risk of fire, vandalism, and accidental damages.
- c. They are brittle and do not show a yielding phenomenon.
- d. These are not strong in the transverse direction of the fibers.
- e. They have a low modulus of elasticity in comparison to steel.

Various Available Forms of CFRPs

a. Carbon Fiber fabrics or textiles

Carbon fiber fabric is similar to other materials other than that it is made of carbon fiber in place of cotton, nylon, or other threads (Figure 1.1). Carbon fiber fabrics are available in different weaves suitable for various applications. For example, a standard twill weave can be used as an all-purpose fabric. Unidirectional fabrics are suitable for strengthening and stiffening in one direction. Carbon fiber fabrics are soft and pliable and need binders to make them rigid. These fabrics are applied in desired shapes, and binders are put in and cured.

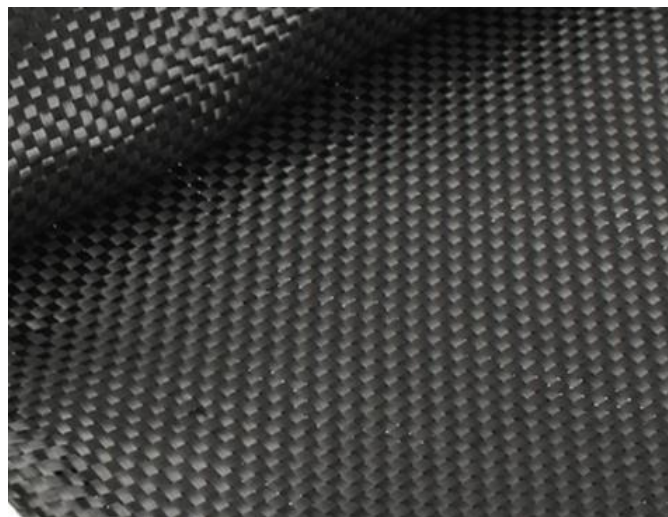


Figure 1.1 CFRP Fabric.

b. Carbon Fiber Sheets and Plates

Carbon fiber sheets are multiple laminations of carbon in an epoxy matrix (Figure 1.2). Generally, unidirectional laminates of fibers are piled up in predetermined order, direction, and thickness to get the required strength and stiffness. These are available in various sizes, weaves, and thicknesses. Carbon fiber plates are considered suitable replacements for aluminum and steel in the industry because of their lightweight and high strength.



Figure 1.2 CFRP Plates.

c. Carbon Fiber Rods

Carbon fiber rods are produced by pulling carbon fibers mixed with binding resins through a heated die (Figure 1.3). The rods have a high stiffness-to-weight ratio, linear strength, and low thermal expansion coefficient. Carbon fiber rods are available in different sizes and rectangular or round shapes.



Figure 1.3 CFRP rods.

CFRP Strengthening Techniques:

Several techniques of FRP strengthening of structures have been developed so far:

a. Externally Bonded Reinforcement Technique

In Externally Bonded Reinforcement (EBR) method, unidirectional or multidirectional fiber sheets or fabrics are bonded to the tension side of the concrete using adhesives (generally epoxies) after surface preparations as shown in Figure 1.4. EBR can be used for flexural as well as shear strengthening of RC structures. FRP EBRs can be applied as a wet layup, prepreg, or precured system. Studies have shown that EBR considerably increases the strength as well as stiffness of weak structures but is susceptible to premature debonding without full utilization of material strength (Malek et al., 1998; Nguyen et al., 2001; Sharif et al., 1994).

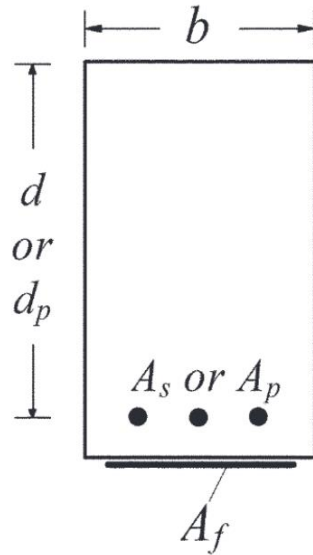


Figure 1.4 EBR strengthening technique (ACI440.2R, 2017).

b. Near-surface-mounted Technique

Another method of FRP strengthening is the Near-surface-mounting (NSM) technique. In NSM methods, grooves are cut on the cover of concrete, where circular or rectangular FRP strips or rods are embedded using epoxy or other adhesives as shown in Figure 1.5. The tensile strength of FRP is better utilized in the NSM method than in the EBR technique. Easier execution, reduced in-situ work, and less exposure to external hazards are some advantages of the NSM technique over the EBR technique (Bilotta et al., 2011; Hawileh, 2012; Lee et al., 2013; Sharaky et al., 2014). NSM performs better than EBR in terms of load-carrying capacity and ductility, but though NSM performs better in terms of debonding issues, debonding and delamination are still the issues (Kotynia, 2012).

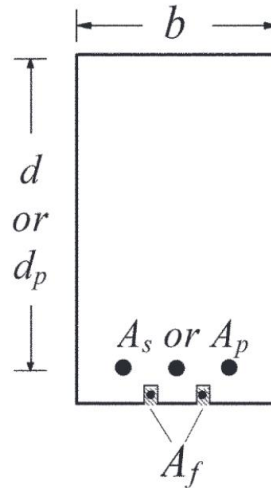


Figure 1.5 NSM strengthening technique (ACI440.2R, 2017).

c. Externally Bonded Reinforcement on Grooves

In externally bonded reinforcement on grooves (EBROG), grooves cut on the concrete were filled with epoxy, and then the FRP was laid over the surface similar to the EBR technique as shown in Figure 1.6. Studies reported that EBROG with longitudinal grooves of suitable width and depth could postpone the premature debonding, and sometimes completely eliminate the premature debonding and lead to FRP rupture as the failure mechanism (Mostofinejad & Hajrasouliha, 2011; Mostofinejad & Kashani, 2013; Mostofinejad & Mahmoudabadi, 2010; Mostofinejad & Shameli, 2011). Providing grooves filled with epoxies increases the contact area between the concrete and epoxy, which helps to transfer more stress and hence delays debonding. EBROG method needs less installation time than the EBR method as surface preparation works are not necessary except for grooving (Mostofinejad & Shameli, 2011).

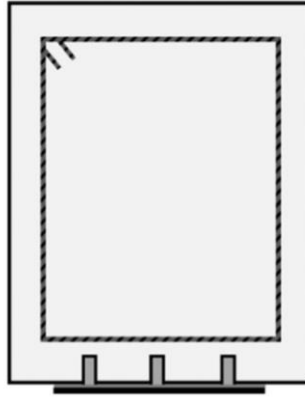


Figure 1.6 EBROG strengthening technique (Mostofinejad & Shameli, 2013)

d. Externally Bonded Reinforcement in Grooves

Externally bonded reinforcement in grooves (EBRIG) is a new FRP strengthening technique introduced by Mostofinejad and Shameli (Mostofinejad & Shameli, 2013). In EBRIG strengthening technique, grooves are cut on the concrete covers, FRP sheets are bonded in such a way that they pass through the internal surface of grooves as shown in Figure 1.7. The grooves are then filled with epoxy materials. Very few studies were carried out on the FRP EBRIG strengthening of concrete beams in flexure and shear (Mostofinejad & Shameli, 2013; Mostofinejad et al., 2014; Shomali et al., 2019, 2020, 2021). (Shomali et al., 2020) reported that diagonal utilization of EBRIG in the beams with and without steel stirrups enhanced the shear capacity by about 60% and 95%, respectively. (Amiri & Talaeitaba, 2020) showed that EBRIG strengthening can increase the punching shear capacity of flat slabs up to 60%. It was reported that EBRIG technique can significantly enhance the flexural load carrying capacity of concrete beams (Mostofinejad & Shameli, 2013; Mostofinejad et al., 2014). The FRP-EBRIG strengthened beams carried 180% and 50% more loads as compared to their corresponding beams strengthened by EBR and NSM

techniques, respectively (Mostofinejad & Shameli, 2013). In addition, the use of EBRIG technique prevented premature debonding of when a single layer of FRP was applied, while debonding was delayed in the case of the beams strengthened by two or three layers of FRP (Mostofinejad & Shameli, 2013; Mostofinejad et al., 2014; Shomali et al., 2021). Studies on EBRIG strengthening of concrete elements are summarized in Table 1.1.

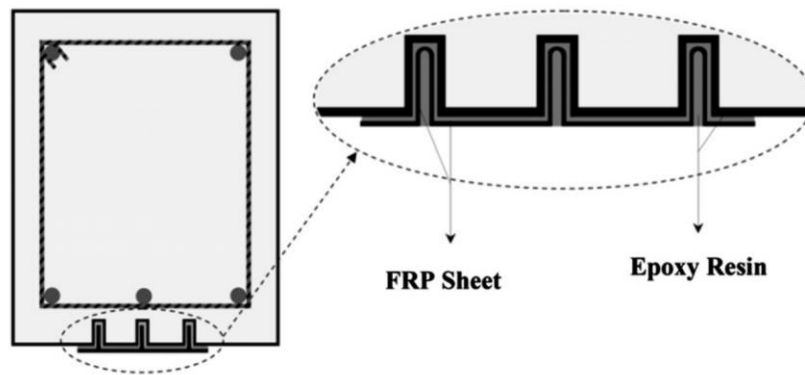


Figure 1.7 EBRIG strengthening technique (Mostofinejad & Shameli, 2013)

Table 1.1 Studies on EBRIG strengthening technique.

S.N.	1	2	3
Reference	(Mostofinejad & Shameli, 2013)	(Mostofinejad et al., 2014)	(Shomali et al., 2019)
Study type	Experimental	Experimental	Experimental
Study element	Concrete beams (1000mm x120mm x140mm)	Reinforced concrete beams (1000mm x120mm x140mm)	Reinforced Concrete beams (2000 mm x200mm x300 mm)
Strengthening Type	Flexural strengthening	Flexural strengthening	Shear strengthening
Longitudinal steel reinforcement	No longitudinal reinforcements.	2 8mm diameter longitudinal tension bars.	3 bottom reinforcements of different size and 2 12 mm top reinforcements.
Transverse steel reinforcement	5 mm stirrups	8 mm diameter stirrups @50 mm	6 mm stirrups at different spacing.
Parameters	Different methods of strengthening with different number of layers of FRP	Different methods of strengthening with different number of FRP layers.	Effect of transverse and longitudinal steel reinforcement ratios on shear strengthening, compressive strength of concrete, orientation of FRP laminates.
Test	Four point bending test	Four point bending test	Four point bending test
Load capacity	Concrete beams with EBRIG strengthening had higher failure load in comparison to other strengthening techniques.	Ultimate load of EBROG2L and EBRIG2L were equal. Ultimate load of EBRIG3L was higher than that of EBROG3L and EBR3L.	EBRIG method of shear strengthening was more effective than EBR method for normal strength concrete.
Failure mode	For both EBROG and EBRIG, FRP ruptured occurred for one layer FRP. For EBROG with multiple layers, the failure mode was interface debonding of FRP. Multilayer EBRIG failed by concrete cover separation.	For both EBROG and EBRIG, FRP ruptured occurred for single layer FRP. For EBROG with multiple layers, the failure mode were concrete cover separation and interface debonding of FRP. Multilayer EBRIG failed by concrete cover separation.	All EBRIG strengthened beams failed with CFRP rupture.
Deformation capacity	EBRIG strengthening had the highest ultimate displacement among the different strengthening techniques.	EBRIG strengthening had the highest ultimate displacement among the different strengthening techniques.	Ultimate displacements of EBRIG strengthened beams were more than that of control beams and beams strengthened by EBR.

Table 1-1 Contd.

S.N.	4	5	6
Reference	(Shomali et al., 2021)	(Shomali et al., 2019)	(Amiri & Talaeitaba, 2020)
Study type	Experimental+Numerical+Analytical	Experimental+Numerical	Numerical
Study element	RC beams (2000mm x200mm x300mm)	RC beams (2000mm x200mm x300mm)	RC Slabs (1220mm x1250 mm x100mm)
Strengthening Type	Shear strengthening	Shear strengthening	Punching shear strengthening
Longitudinal steel reinforcement	3 bottom bars of different sizes, 2 top bars of 12 mm diameter	3 20 mm bottom bars, 2 12 mm top bars	
Transverse steel reinforcement	Either not provided, or 6 mm stirrups provided at 125 and 185 mm spacing.	6 mm stirrups at different spacing	
Parameters	Flexural reinforcement ratios, shear reinforcement ratios	Orientation of EBRIG, stirrup spacing	EBROG and EBRIG method of strengthening, width and depth of grooves, number of FRP layers
Test	Four point bending test	Four point bending test	
Load capacity	Higher peak load was observed in EBRIG shear strengthening.	Higher value for peak load was obtained.	EBROG and EBRIG methods increased the peak load considerably in comparison to EBR.
Failure mode	CFRP rupture was observed in all beams strengthened by EBRIG method.	Rupture of CFRP.	Shear-flexural failures were observed in slabs with EBROG and EBRIG.
Deformation capacity	Higher mid span deflection was observed in EBRIG shear strengthening.	Higher value was obtained for mid-span deflection.	Final displacements of slabs with multiple layers of FRP were less than those of single layered.

Although the studies conducted until now have shown that the EBRIG technique delays or even eliminates the FRP sheets debonding and enhances load capacity of RC beams more than EBR and NSM techniques, further studies on the flexural strengthening of concrete beams by EBRIG have not been conducted extensively. To the best of authors' knowledge, no study has been performed to understand the effect of parameters such as the number and the depth of grooves on the flexural behavior of RC beams strengthened with EBRIG technique. The present paper investigates the flexural strengthening by externally bonded reinforcement in groove (EBRIG) of reinforced concrete (RC) beams using various layers of carbon fiber reinforced polymers (CFRP). ANSYS Mechanical APDL software was used to model the beams which were validated through an existing experimental study in the literature. Subsequently, a detailed parametric study was performed to analyze the effect of various groove number and depths on the performance of EBRIG strengthened RC beams with single, double, or triple layers of CFRP. Additionally, the beams were strengthened by combining EBRIG and near surface mounting (NSM) technique, for which NSM FRP bar size was also investigated.

1.2 Methodology

3D models of beams were created in ANSYS Mechanical APDL 2020 R2 using graphical user interface as well as APDL codes. Due to the symmetry, half of the beam was modeled to reduce the computational time. Suitable element types and material properties were assigned for the concrete, steel reinforcement bars and plates, CFRP bars and sheets, and epoxy materials. The displacement control loads were applied, and Newton-Raphson method was employed to execute the non-linear static finite element analysis. The output

of the analysis results were investigated in terms of ultimate load carrying capacity, ultimate mid-span displacement, load versus displacement curves, and the failure modes.

1.3 Chapter 2 Summary

In this study, four experimental beams of study were used to validate the FEA beams. This chapter discusses the geometry and materials of those selected beams.

1.4 Chapter 3 Summary

In this chapter, the finite element analysis approach applied for modeling and analysis of the beam model are discussed. The element types and material models adopted for the concrete, steel rebars and plates, CFRP sheets and rods, and epoxy materials are described in this chapter. Also, the boundary conditions and failure criteria are discussed in this chapter.

1.5 Chapter 4 Summary

This chapter describes the validation of the FEA beam models. The load displacement curves, ultimate loads, ultimate displacements, and failure modes of the FEA beam modes and the corresponding experimental beams are discussed.

1.6 Chapter 5 Summary

Chapter 5 presents the parametric study. The parameters considered were the depth and number of grooves in EBRIG strengthened beams. Additionally, the beams were strengthened by combining EBRIG and near-surface mounting (NSM) technique, for

which NSM FRP bar size was also investigated. The performance of the beam models were studied in terms of ultimate loads, load versus displacement curves, and the failure modes.

1.7 Chapter 6 Summary

This chapter summarizes all the findings and conclusions of the thesis.

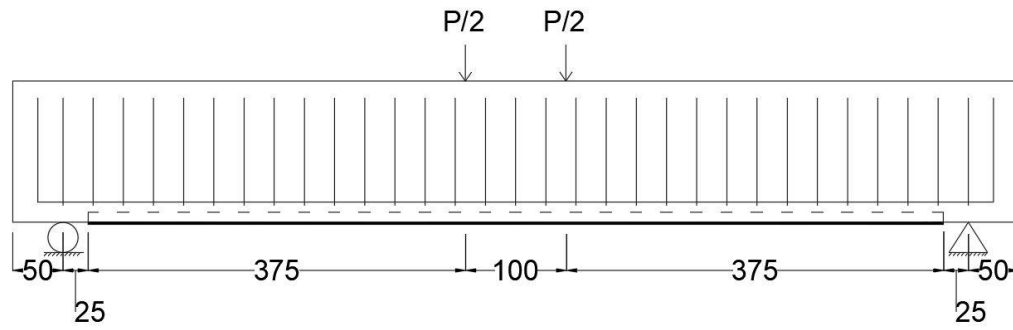
1.8 Chapter 7 Summary

This chapter presents recommendations based on the current study and possible areas for future studies.

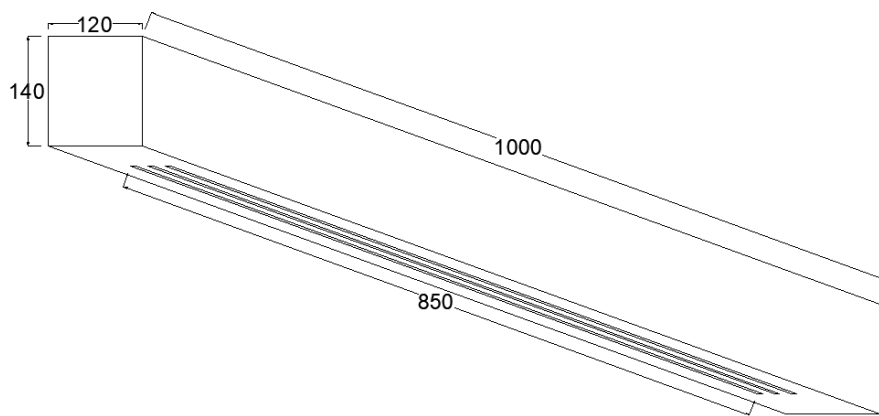
Chapter 2

Experimental Study for the Validation of FEA Beam Models

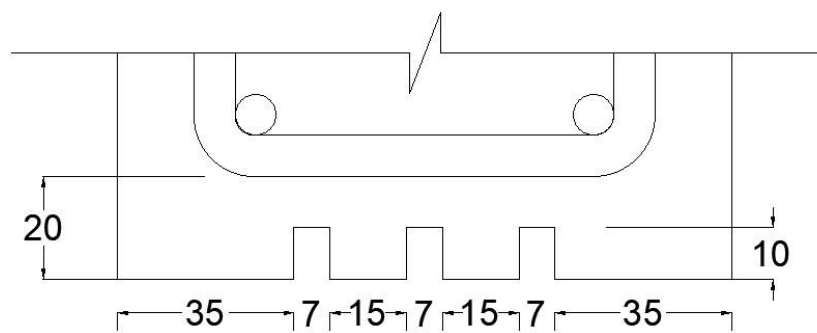
An existing experimental study (Mostofinejad et al., 2014) was used to validate the FEA beam models CB (control), S1, S2, and S3 (EBRIG strengthened with one, two, and three layers of CFRP sheets, respectively). The tested beams were 1000 mm length, 120 mm width and 140 mm height subjected to four-point loading tests. The scale-down beams were chosen because only limited experimental study have been conducted on this method, and all the experiments have used only scale-down RC beams. 8 mm diameter steel bars were used for both longitudinal as well as transverse reinforcement. Compressive strength of concrete of tested beams ranged between 33 and 37 MPa. The yield strength of the flexural and shear reinforcement was 530 MPa. The clear covers for the steel reinforcements in the beams were 20 mm. For the strengthened beams, three grooves of 850 mm length, 7 mm width and 10 mm depth were carved at the beam bottom at spacing of 15 mm. Sika Wrap Hex230C carbon fibers sheets of length 850 mm, width 100 mm, and thickness 0.12 mm with an elastic modulus of 230 GPa and ultimate tensile strain of 0.017 were applied at all sides of the grooves using epoxy. Sikadur C31 epoxy resin with a tensile modulus of 5200 MPa and tensile strength of 24.8 MPa was used as the filler material in those grooves after the application of CFRP. The dimensions, reinforcement, and groove details of the beams are also shown in Fig. 2.1.



(a)



(b)



(c)

Figure 2.1 (a, b and c)

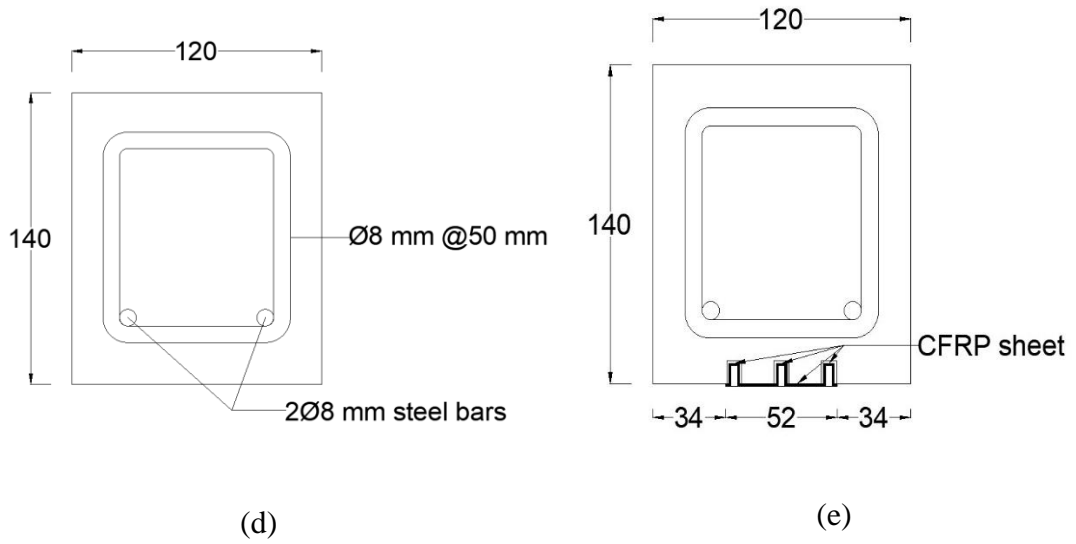
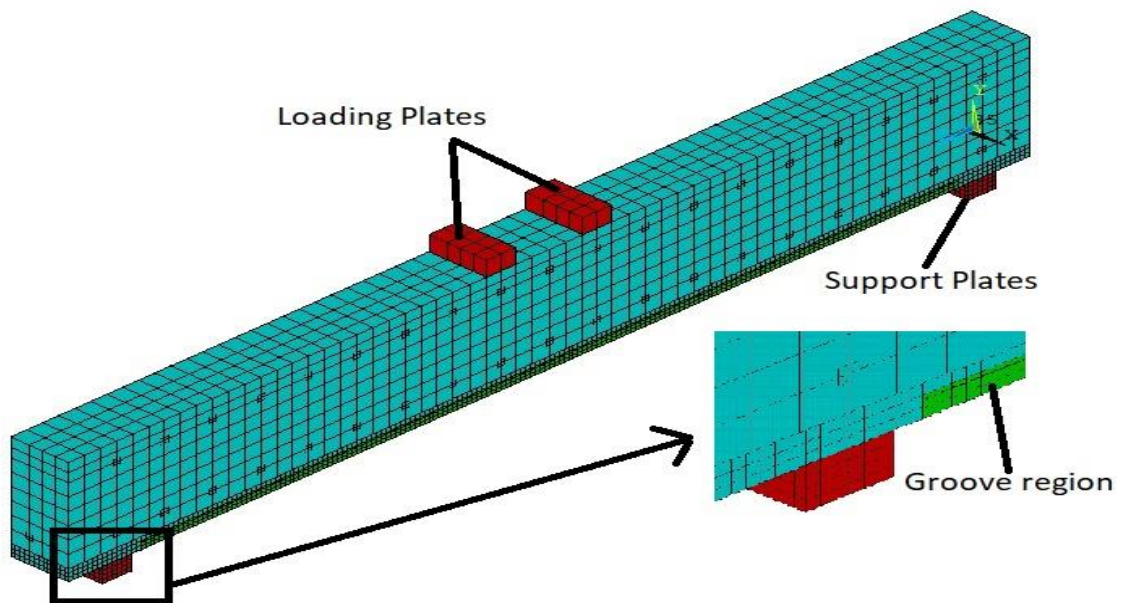


Figure 2.1(d and e) Schematic view of the beam: (a) side view, (b) 3-D view, (c) size and spacing of grooves (d) cross-section view of CB, (e) cross-section view of S1, S2 and S3. (all dimensions are in mm)

Chapter 3

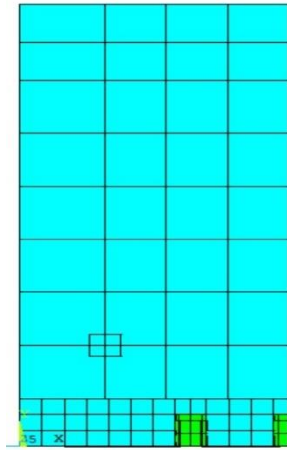
Finite Element Analysis Approach

3D models of beams were created in ANSYS Mechanical APDL 2020 R2 using graphical user interface as well as APDL codes as shown in Figure 3.1. Due to the symmetry, half of the beam was modeled to reduce the computational time. The element types, material models, boundary conditions, non-linear analysis and failure modes are defined in the following sections:

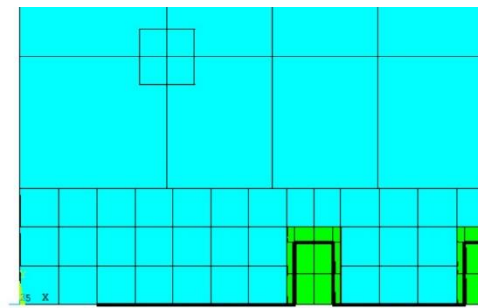


(a)

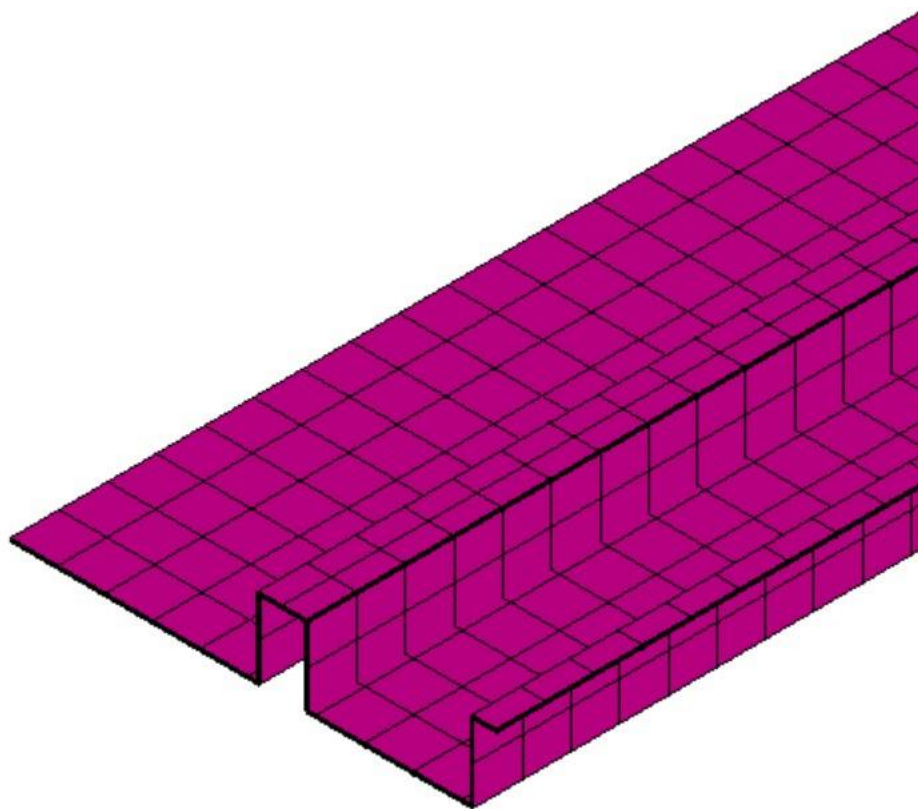
Figure 3.1 (a)



(b)



(c)



(d)

Figure 3.1(b, c and d) FE Models of Beam (a) 3D view, (b) Cross-section view, (c) Cross-section view, and (d) CFRP sheets in FEA models

3.1 Element Types

3.1.1 Concrete

Concrete was modeled using SOLID65 element which is a linear brick element defined by eight nodes. Each node has three translational degrees of freedom. The element can capture cracking, crushing, creep, large deflection, large strain, and stress stiffening (ANSYS, 2020). The geometry of the element are depicted in Figure 3.2.

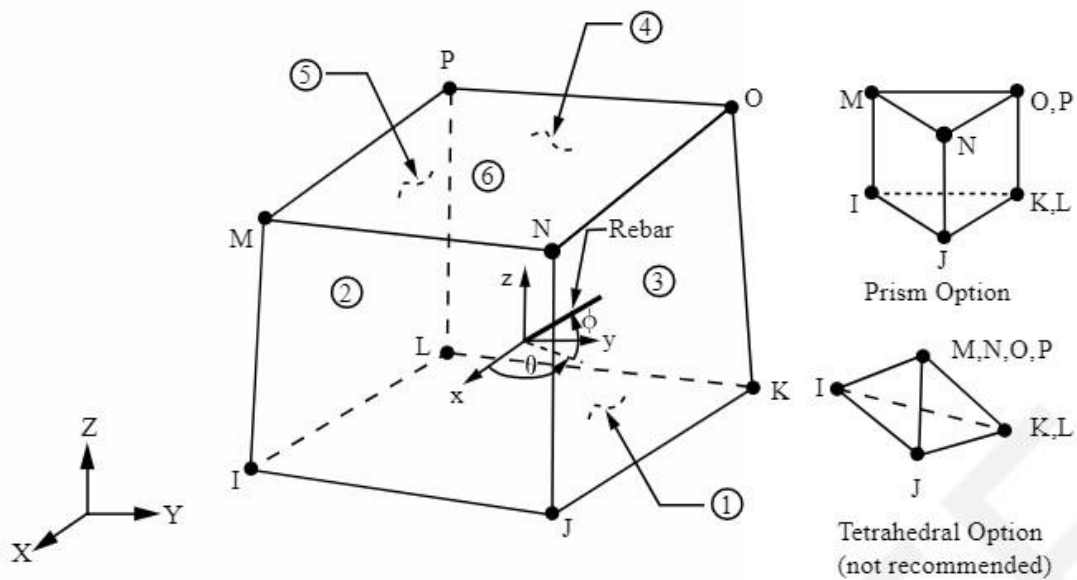


Figure 3.2 Solid65 (ANSYS, 2020).

3.1.2 Steel and FRP bars

Reinforcement bars can be modeled in FE by three different approaches-smeared rebar approach, embedded rebar approach, and discrete rebar approach as depicted in Figure 3.3 (Chong, 2004; Tavárez, 2001). In smeared approach, the reinforcement is uniformly distributed in base element, where the material property is formed from individual properties of base and reinforcement materials by composite principal. In embedded approach, rebar is embedded in base element without sharing nodes. In discrete model, link, truss or beam elements are used as rebar which share the node with the base elements.

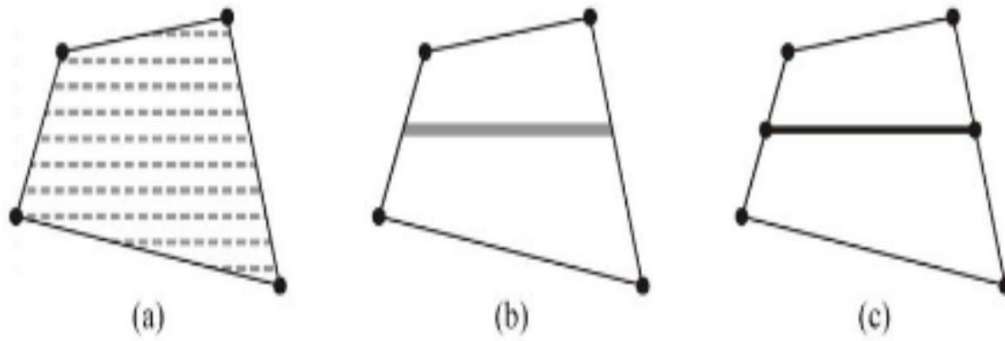


Figure 3.3 Rebar modelling approaches: (a) smeared approach, (b) embedded approach, and (c) Discrete Approach (Chong, 2004).

In this study, steel and FRP reinforcement bars were modeled by discrete approach using Link180 element (Fanning, 2001). LINK180 element is a 3-D tension-compression element with two nodes each having three translational degrees of freedom. The element can capture plasticity, creep, large deflection and is generally used to model bars, springs, links, and cables (ANSYS, 2020). The geometry of the element are depicted in Figure 3.4.

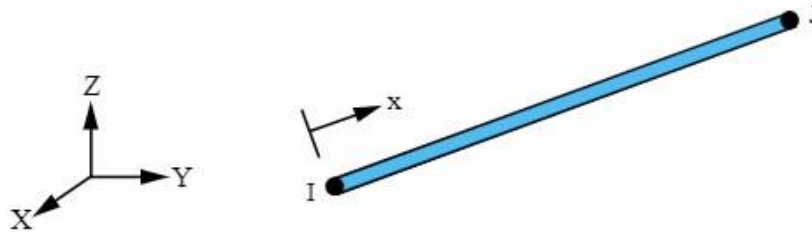


Figure 3.4 LINK180 (ANSYS, 2020).

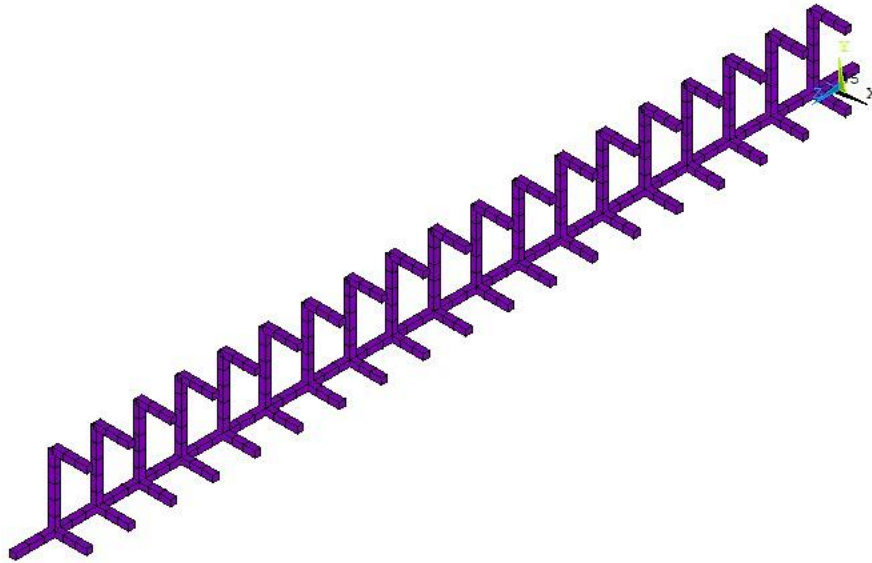


Figure 3.5 Steel reinforcement bar elements in FEA beam model.

3.1.3 FRP Sheets

SHELL181 element which is suitable to model layered composite shells were used to model the Carbon fiber sheets. SHELL181 element comprises of four nodes each having six degrees of freedom. Membrane option of SHELL181 uses three translational degrees of freedom only (ANSYS, 2020). The geometry of the element is depicted in Figure 3.6.

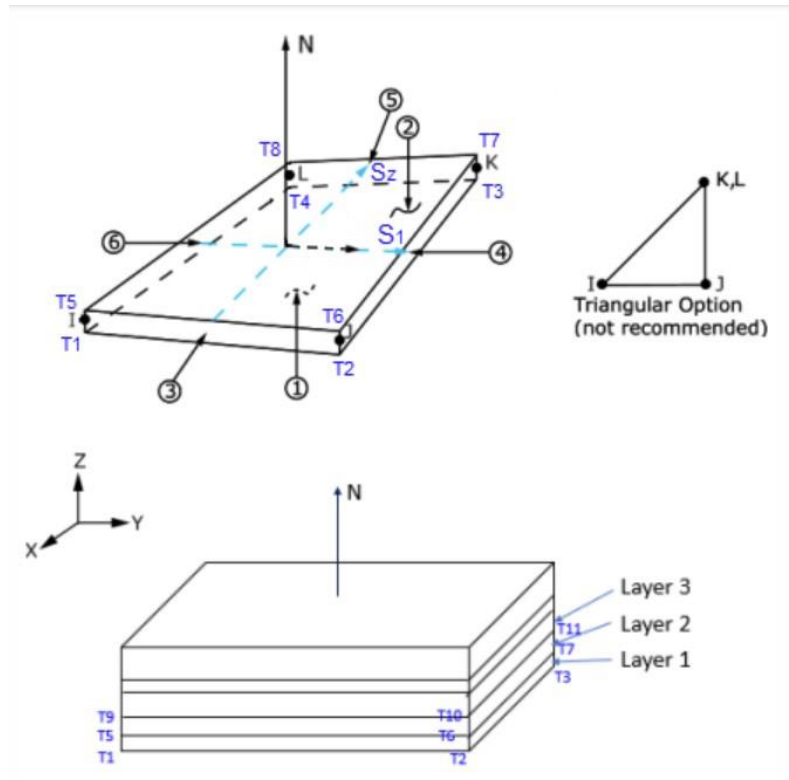


Figure 3.6 SHELL 181 (ANSYS, 2020).

3.1.4 Steel Plates and Epoxy Materials

The steel plates at the supports and loading positions, and the epoxy materials used for filling the grooves were modeled using SOLID185. SOLID185 is a 3-D solid element defined by eight nodes each having three translational degrees of freedom. The element can model both homogeneous as well as layered solids (ANSYS, 2020). The geometry of the element are depicted in Figure 3.7.

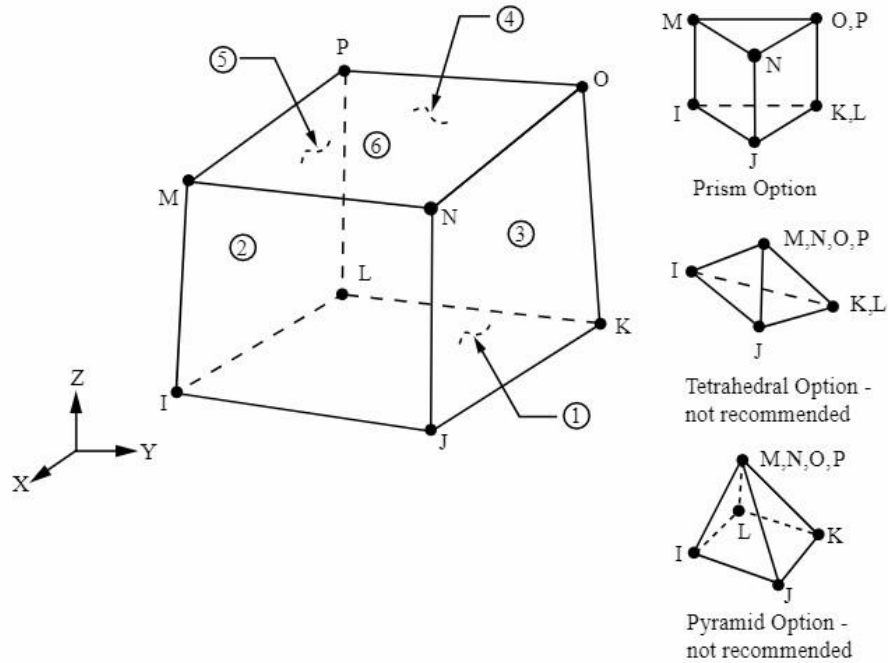


Figure 3.7 SOLID185 (ANSYS, 2020).

3.1.5 Element Interfaces

The concrete-epoxy interface and concrete-FRP sheet interface were modeled by surface-to-surface contact pairs TARGET170 and CONTA174. TARGET170 is used to simulate various 3D surfaces for associated contact elements. CONTA174 can simulate contact and sliding at the interface surfaces (ANSYS, 2020). The interfacial surfaces of concrete were simulated by TARGET170, and the interfacial surfaces of epoxy or CFRP sheets were simulated by CONTA174. The geometry of TARGET170 and CONTA174 are depicted in Figure 3.8 and Figure 3.9 respectively.

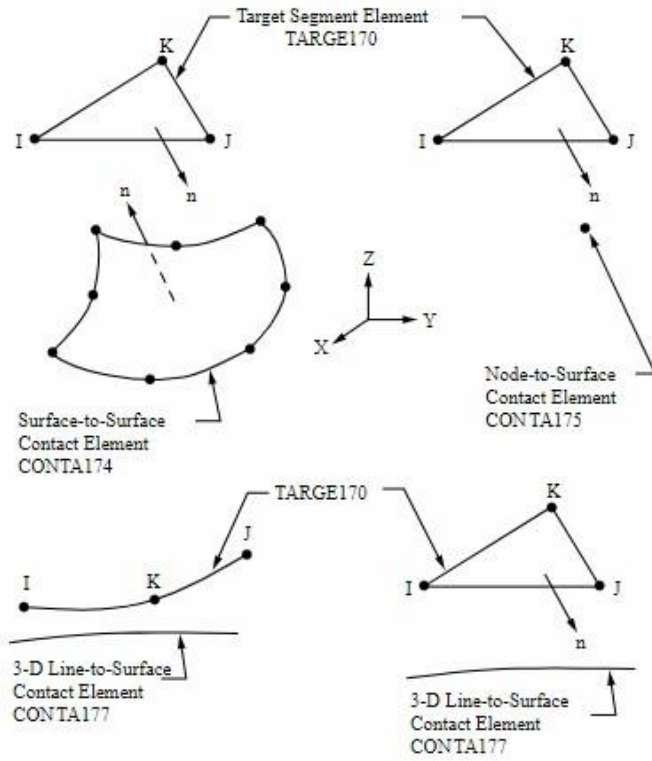


Figure 3.8 TARGET170 (ANSYS, 2020).

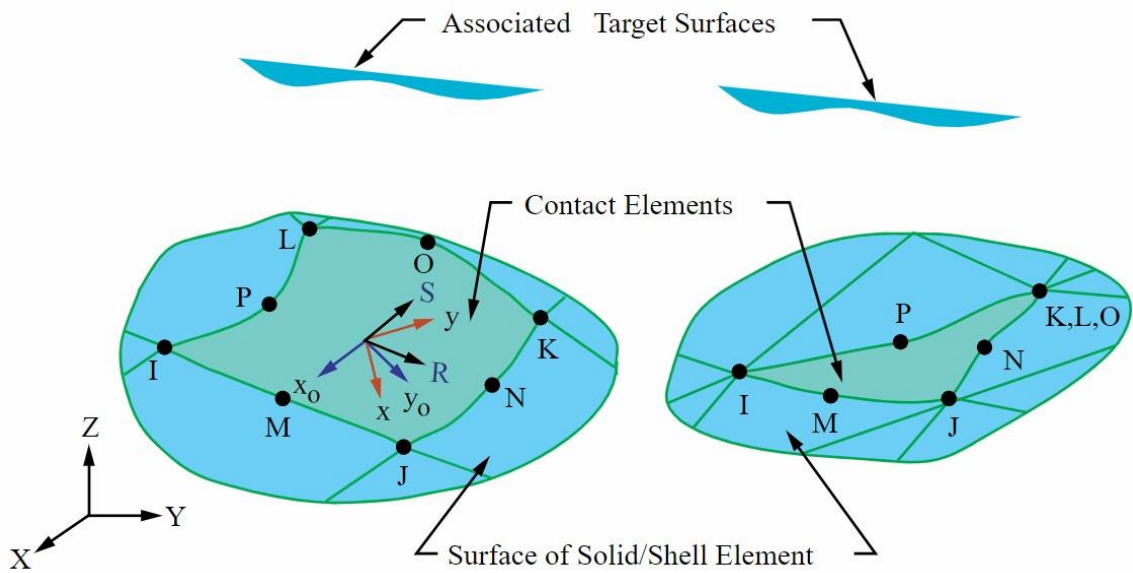


Figure 3.9 CONTA174(ANSYS, 2020).

3.2 Material Models

3.2.1 Concrete

Concrete was modeled by linear and multi-linear isotropic material properties in combination with concrete model predefined in ANSYS. The stress-strain curve of concrete in both compression and tension were defined. The linear elastic properties of concrete were defined by elastic modulus (E_c) and poisson's ratio (μ_c). The elastic modulus of concrete was approximated using Eq. 3.1 as follows (ACI318, 2019):

$$E_c = 4700\sqrt{f'_c} \quad \text{Eq. 3.1}$$

where f'_c is the compressive strength of the concrete. Poison's ratio of concrete was assumed to be 0.2 (Bangash, 1989).

Several analytical models are available to estimate the stress versus strain curve behavior of concrete in compression (Desayi & Krishnan, 1964; Hognestad et al., 1955; Model Code, 2010; Thorenfeldt, 1987; Todeschini et al., 1964). In this study, the behavior of concrete in compression was defined using hognested curve (Hognestad et al., 1955) given by Eqs. 3.2 and 3.3 as follows:

$$f_c = f'_c \left[2 \left(\frac{\varepsilon}{\varepsilon_0} \right) - \left(\frac{\varepsilon}{\varepsilon_0} \right)^2 \right] \quad \text{Eq. 3.2}$$

$$\varepsilon_0 = \frac{2f'_c}{E_c} \quad \text{Eq. 3.3}$$

where f_c is the compressive stress in concrete at strain ε , and ε_0 is the strain corresponding to f' . The behavior of concrete was assumed to behave perfectly plastic after reaching the

compressive strength as shown in Fig. 3.10 due to the inapplicability of a negative slope in the stress versus strain curve in ANSYS (ANSYS, 2020) . Similar approach was used by (Jia, 2003; Kachlakev et al., 2001).

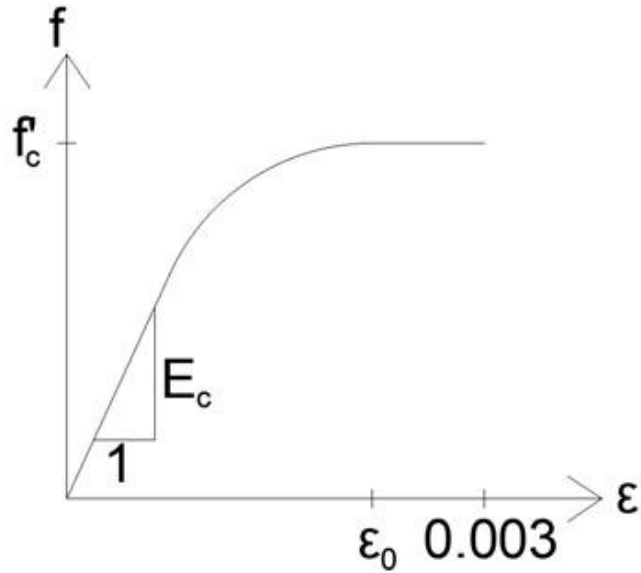


Figure 3.10 Stress versus strain curve of concrete under compression.

Linear elastic behavior was assumed for the concrete in tension up to rupture at ultimate tensile stress (f_t) followed by softening as shown in Figure 3.11 . The tensile strength (f_t) of concrete were approximated using Eq. 3.4. The softening was modeled by sudden drop in tensile stress by 40%, after which the stress decay linearly to 0 at $6\epsilon_t$ as predefined in ANSYS.

$$f_t = 0.6\sqrt{f'_c} \quad \text{Eq. 3.4}$$

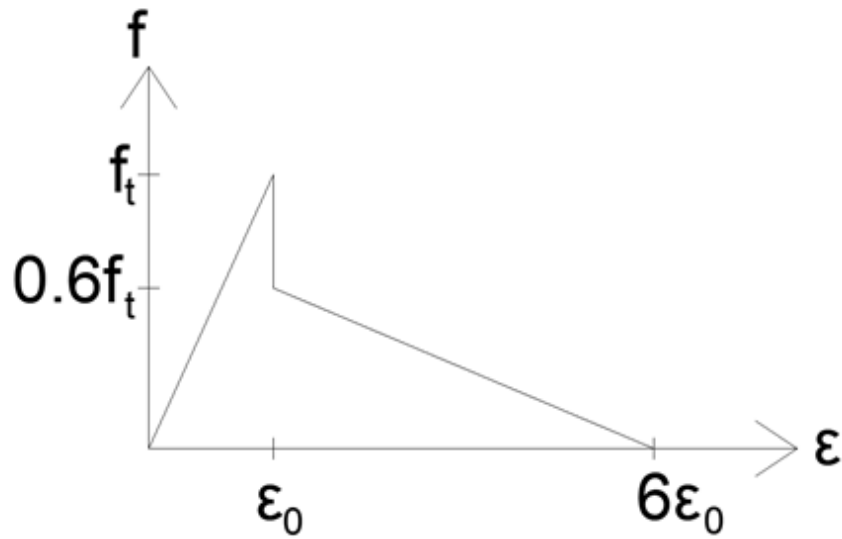


Figure 3.11 Stress-strain curve of concrete under tension.

Concrete material model (CONCR) available in ANSYS (ANSYS, 2020) was employed to predict the failure of concrete by cracking or crushing. This material model which is based on William and Warnke failure criteria (Willam, 1975) is defined by at least four parameters- tensile cracking stress (f_t), uniaxial crushing stress (f'_c), and open and closed shear transfer coefficients. In this material model, concrete cracking occurs when the principal stress reaches tensile cracking stress (f_t). The crushing capability of concrete was deactivated by applying a value of -1 for uniaxial crushing stress as recommended by ANSYS to avoid the premature failure due to high stress concentration near loading and support plates. Similar approach was adopted by (Chansawat et al., 2006; Jia, 2003; Kachlakev et al., 2001; Omran & El-Hacha, 2012; Willam, 1975; Wolanski, 2004). When crushing capability of concrete is deactivated, beam failure occurs by cracks induced by the secondary tensile strain due to Poisson's effect (Kachlakev et al., 2001). The value of

shear transfer coefficients ranges between 0 and 1, where 0 represents smooth crack and 1 represents a rough crack (ANSYS, 2020). In this study, a value of 0.2 was used for both the open and close shear coefficients based on sensitivity analysis. Similar value for shear transfer coefficients were used by (Hawileh, 2012).

3.2.2 Steel

Elastic-perfectly plastic material model was used to simulate the behavior of steel reinforcement bars as shown in Fig.3.12 (Neale et al., 2005). Poisson's ratio and elastic modulus of steel were assumed to be 0.3 and 200 GPa, respectively.

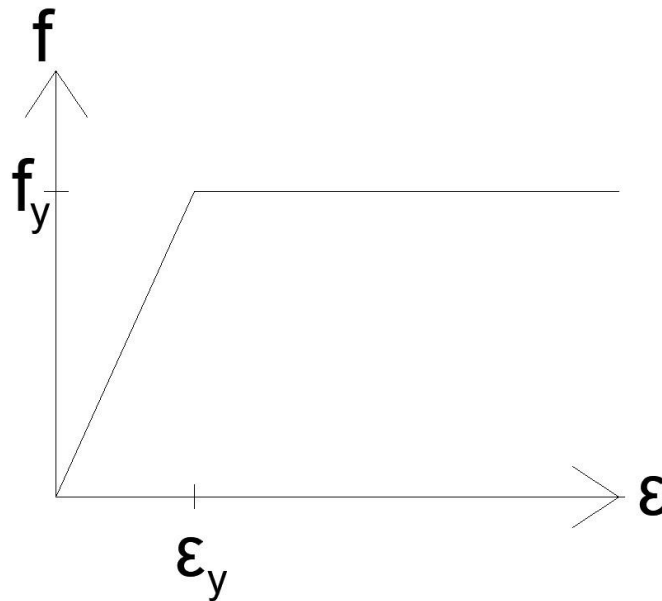


Figure 3.12 Stress versus strain curve of steel reinforcement bars.

3.2.2. CFRP

CFRP materials are the composites formed by embedding high strength carbon fibers in polymer matrix. The carbon fibers contribute to the high strength and stiffness of the composite in the direction of fibers. The matrix, which act as binding agent for the fibers, have negligible contribution in composite strength and stiffness. Hence, CFRPs are orthotropic materials with very high strength and stiffness only in the direction of fibers. The basic composition of CFRP is illustrated in Figure 3.13. Linear anisotropic material property was defined for the CFRP materials by assigning the elasticity only in the direction of the fibers as shown in Figure 3.14.

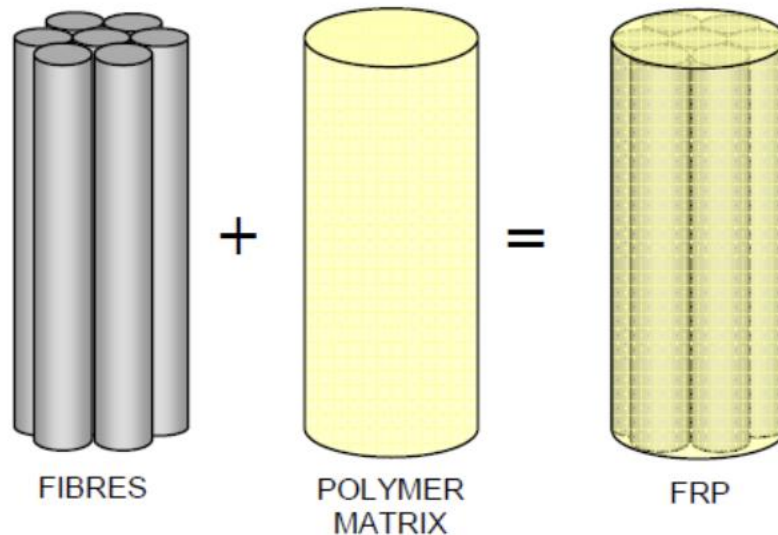


Figure 3.13 Composition of CFRP composites (Kaw, 2006).

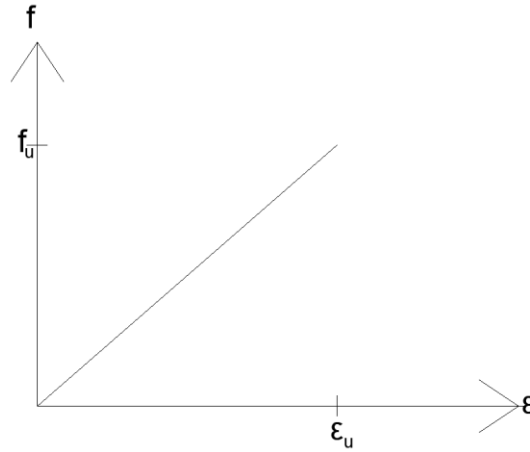


Figure 3.14 Stress versus strain curve of CFRP in the direction of fiber.

3.2.3. Epoxy Materials

Sikadur C31, which was used to fill the grooves after the application of the CFRPs, were modeled as multilinear elastic isotropic material. The stress versus strain curve assigned for the epoxy material is shown in figure. Similar approach was used by (Omran & El-Hacha, 2012) to define the epoxy material behavior.

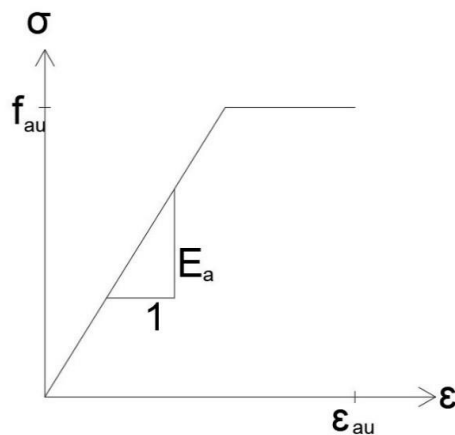


Figure 3.15 Stress versus strain curve of epoxy material.

3.2.4. Cohesive Zone Materials

The FRP-concrete interface at the bottoms of the beams, and the concrete-epoxy interface were modeled by cohesive zone material models with bilinear behavior.

Bilinear bond slip relation was assigned for the concrete-FRP interface at the bottom of the beam, defined by Eqs. 3.5 to 3.11 as follows (Lu et al., 2005):

$$\tau = \tau_{max} \frac{s}{s_0} \text{ if } s \leq s_0 \quad \text{Eq. 3.5}$$

$$\tau = \tau_{max} \frac{s_f - s}{s_f - s_0} \quad \text{Eq. 3.6}$$

$$s_f = \frac{2G_f}{\tau_{max}} \quad \text{Eq. 3.7}$$

$$s_0 = 0.0195\beta_w f_t \quad \text{Eq. 3.8}$$

$$\tau_{max} = 1.5\beta_w f_t \quad \text{Eq. 3.9}$$

$$G_f = 0.308\beta_w^2 \sqrt{f_t} \quad \text{Eq. 3.10}$$

$$\beta_w = \sqrt{\frac{2.25 - \frac{b_f}{b_c}}{1.25 + \frac{b_f}{b_c}}} \quad \text{Eq. 3.11}$$

where τ is local bond stress, s is local slip, τ_{max} is the maximum local bond stress, s_0 is slip corresponding to τ_{max} , s_f is ultimate slip, G_f is interfacial fracture energy, β_w is width ratio factor, b_f is the width of FRP sheet, and b_c is the width of concrete.

The concrete-epoxy interface was modeled using contact pairs and cohesive zone model. Mixed-mode debonding was employed which includes both shear stress-slip and stress-gap models. The shear stress-slip model is defined by Eqs. 3.12 to 3.15 as follows (Seracino et al., 2007):

$$\tau_{tmax} = (0.802 + 0.078\varphi)f'_c{}^{0.6} \quad \text{Eq. 3.12}$$

$$G_{ct} = \frac{0.976\varphi^{0.526}f'_c{}^{0.6}}{2} \quad \text{Eq. 3.13}$$

$$u_t^c = \frac{0.976\varphi^{0.526}}{0.802 + 0.078\varphi} \quad \text{Eq. 3.14}$$

$$\varphi = \frac{\text{groove depth} + 1}{\text{groove width} + 2} \quad \text{Eq. 3.15}$$

where τ_{tmax} is the maximum shear contact stress, φ is the groove aspect ratio, G_{ct} is the shear fracture energy, u_t^c is ultimate contact slip.

The contact gap model was defined by Eqs. 3.16 to 3.18 (Omran & El-Hacha, 2012) as follows:

$$\sigma_{max} = f_t \quad \text{Eq. 3.16}$$

$$G_{cn} = G_{fo} \left(\frac{f'_c}{10} \right)^{0.7} \quad \text{Eq. 3.17}$$

$$u_n^c = G_{fo} \left(\frac{\sqrt{10} f'_c}{24.3} \right)^{0.2} \quad \text{Eq. 3.18}$$

where σ_{max} is maximum contact stress, G_{cn} is total fracture energy, u_n^c is contact gap, and G_{fo} is the base value of fracture energy. G_{fo} which depends on size of maximum aggregate size, was approximated to be 0.034 N/mm (USDOT, 2007) .

3.3. Boundary Conditions

All beams were subjected to four point bending tests. Hinge supports were provided by restricting the displacements of nodes of support plate in the longitudinal and vertical direction of the beams. Roller supports were provided by restricting displacement of support plates in vertical direction. Displacement control load was applied, where non-zero displacements were applied on the loading plates in the direction of loads. The reactions at the nodes were evaluated to get the external loads being applied on the beams. Loads and supports are shown in Figure 3.16. Since only half of the beams were modeled, displacements of the nodes in direction of plane of symmetry were restrained as shown in Figure 3.17.

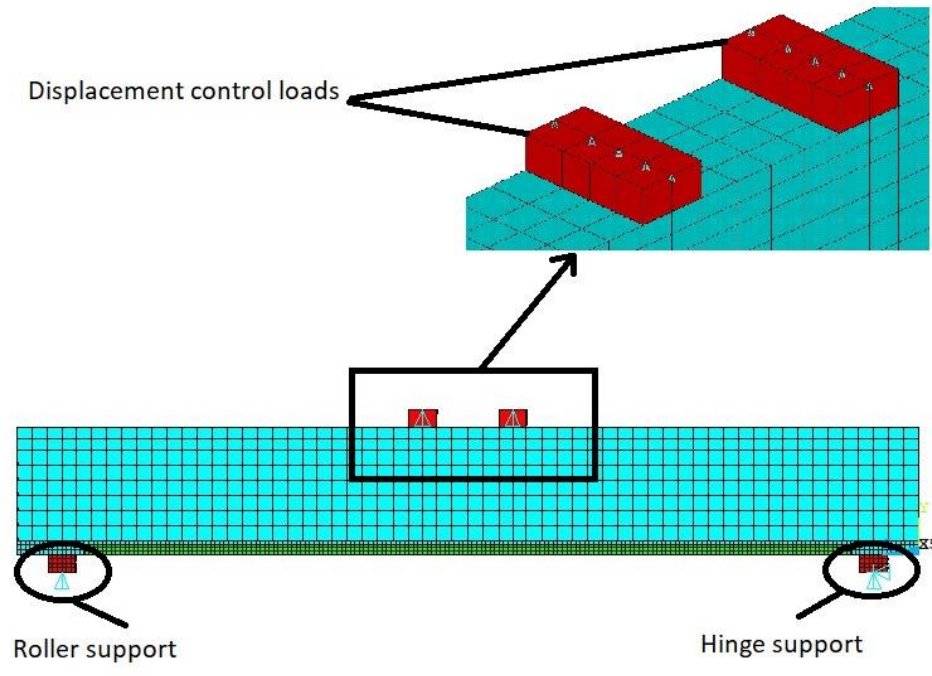


Figure 3.16 Supports and loadings in FEA models.

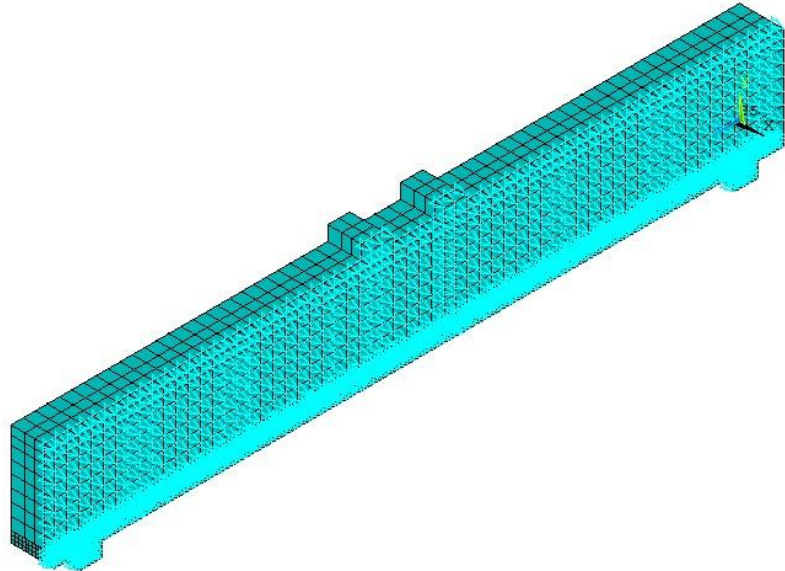


Figure 3.17 Symmetry boundary condition.

3.4. Nonlinear Analysis and Failure Modes

Displacement control method was applied to perform the nonlinear solution. In non-linear method, the non-zero displacement are applied at the position and direction of the loads, and the loads being applied on the model are evaluated in terms of reaction forces at those non-zero displacement constraints. Newton-Raphson method was employed to execute the non-linear static finite element analysis. Following criteria are considered for the failure of the beam in this study (ACI440.2R, 2017):

- a. concrete crushing compressive strain of 0.003,
- b. FRP rupture as the fabric reaches failure strain, and
- c. concrete cover separation when the substrate cannot withstand the force in FRP.

Chapter 4

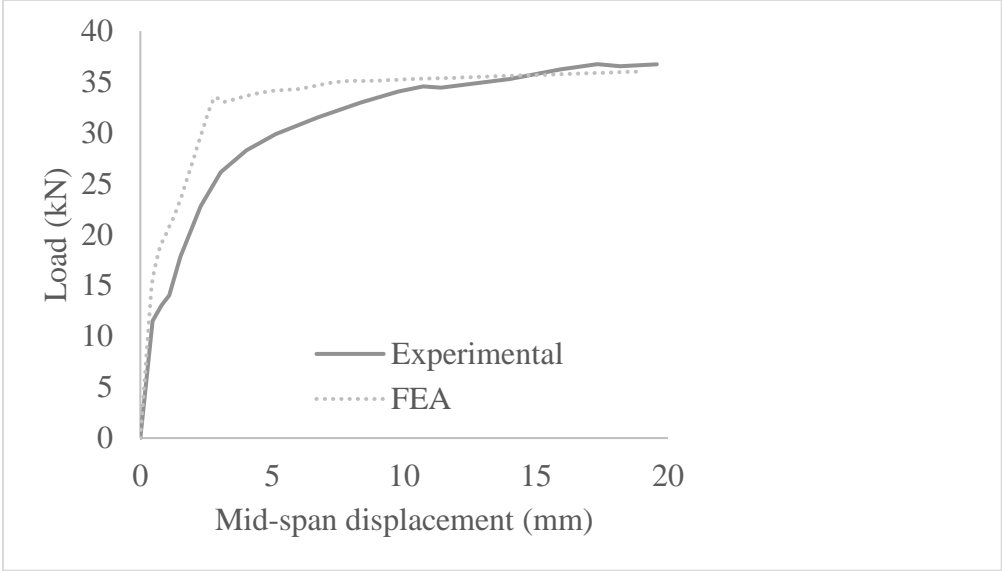
Validation of FEA Beam Models

The results of finite element analysis and experimental results were in good agreement with less than 8% discrepancy in ultimate load and mid-span displacement. The peak loads, mid-span displacement and the failure modes of FE beam models and experimental beams (Mostofinejad et al., 2014) are shown in Table 4.1. The comparison of load versus displacement curves of the experimental beams (CB, S1, S2 and S3) and corresponding FEA models are shown in Table 4.1.

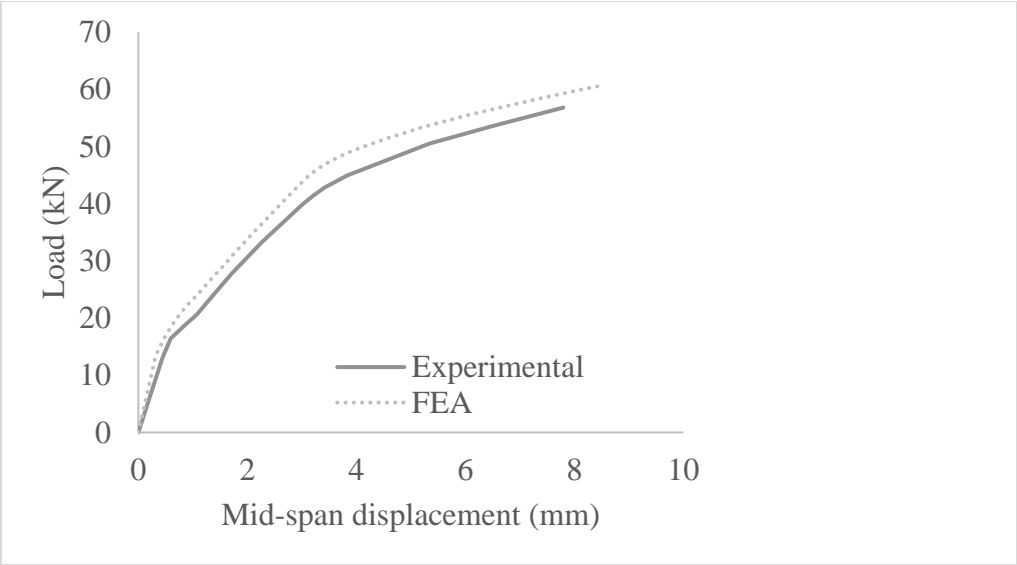
Table 4.1 Comparison of experiment and FEM results

Beam ID	No. of CFRP Layers	Experiment		FEA		Discrepancy		Failure Mode
		P (kN)	Δ (mm)	P (kN)	Δ (mm)	P (%)	Δ (%)	
CB	–	36.7	19.1	36	19.6	2	2.4	Rebar yielding
S1	1	56.8	7.8	60.5	8.4	6.6	8.2	concrete cover separation
S2	2	75.3	10.4	80.5	9.9	6.9	4.9	concrete cover separation
S3	3	83.2	9.8	88.8	9.4	6.8	4.5	concrete cover separation

P: Load, Δ : Mid-span displacement

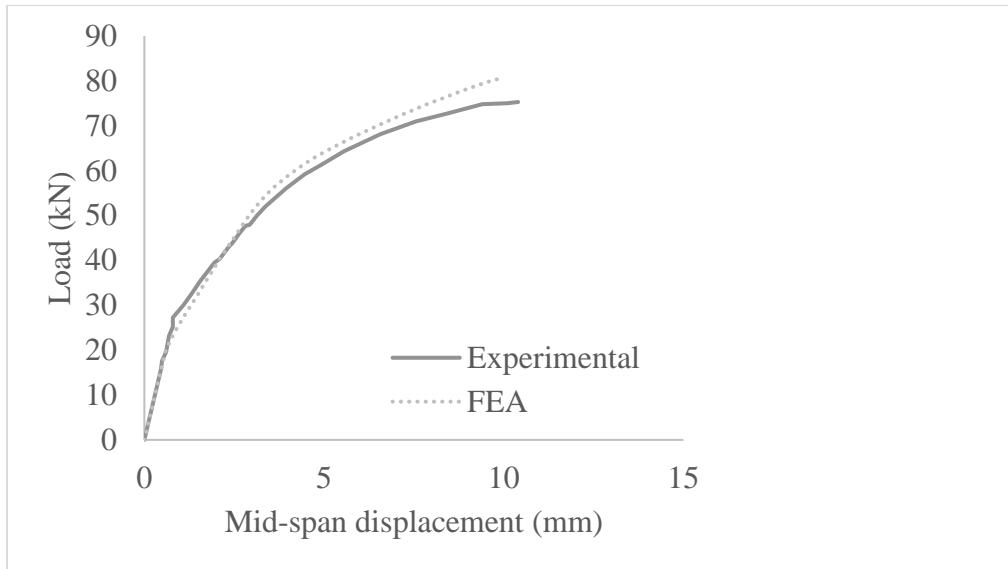


(a)

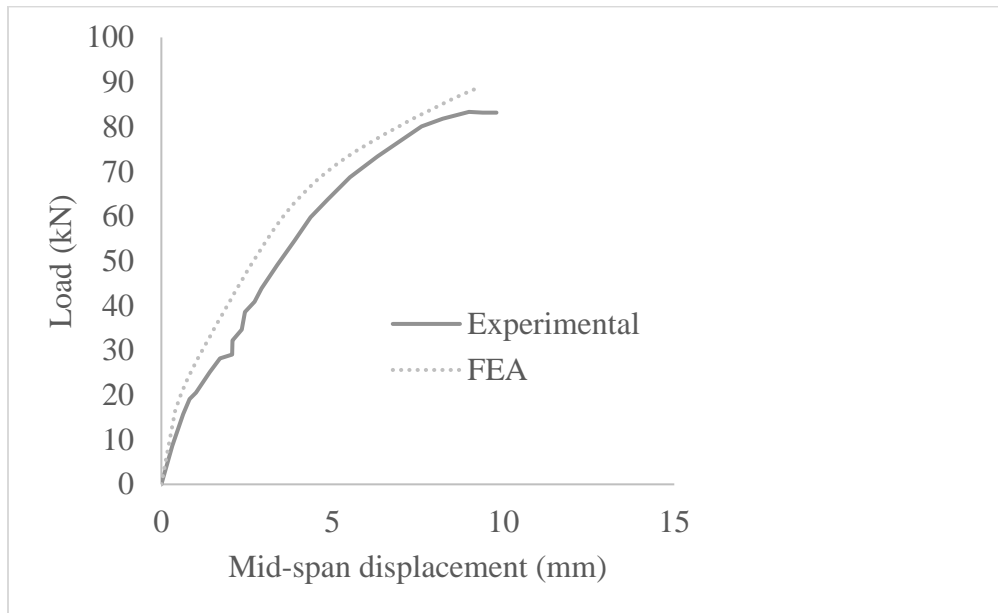


(b)

Figure 4.1 (a and b)



(c)



(d)

Figure 4.1 (c and d) Load versus displacement curves of experimental and FEA of (a) CB beam, (b)S1 beam, (c) S2 beam, and (d)S3 beam.

Chapter 5

Parametric Study

After validating the FE beam models, a parametric study on CFRP EBRIG strengthened beams was carried out to investigate the effect of various groove depths, groove numbers, and strengthening techniques. Additionally, strengthening of beams using combination of EBRIG and NSM rods were also studied. In the experiment, FE beam models that were validated with the experiment (Mostofinejad et al., 2014), the CFRP sheets had a constant length of 850 mm and a width of 100 mm which was extended up to 34 mm away from both beam's edges [Fig. 2 (a)]. For the parametric study, new beam models were developed where the FRP sheets were extended up to 10 mm from both edges of the beams [Fig. 11 (a)]. The beams were labeled as L#-GD#-GN# where the symbol # appearing after L, GD, and GN represent the number of CFRP layers, groove depth, and the numbers of grooves, respectively. For example, L1-GD10-GN3 represents the beam strengthened by the EBRIG technique with a single layer of CFRP sheet and three grooves of 10 mm depth. To investigate the effect of combining EBRIG strengthening technique with NSM rod, CFRP rods with various sizes were installed in the grooves as shown in Fig. 11(b). The beams strengthened by combined CFRP EBRIG-NSM rods were designated as L#-GD#-GN#- ϕ #, where ϕ represents the diameter of NSM FRP rods. The details of the parametric study are presented in the following sections.

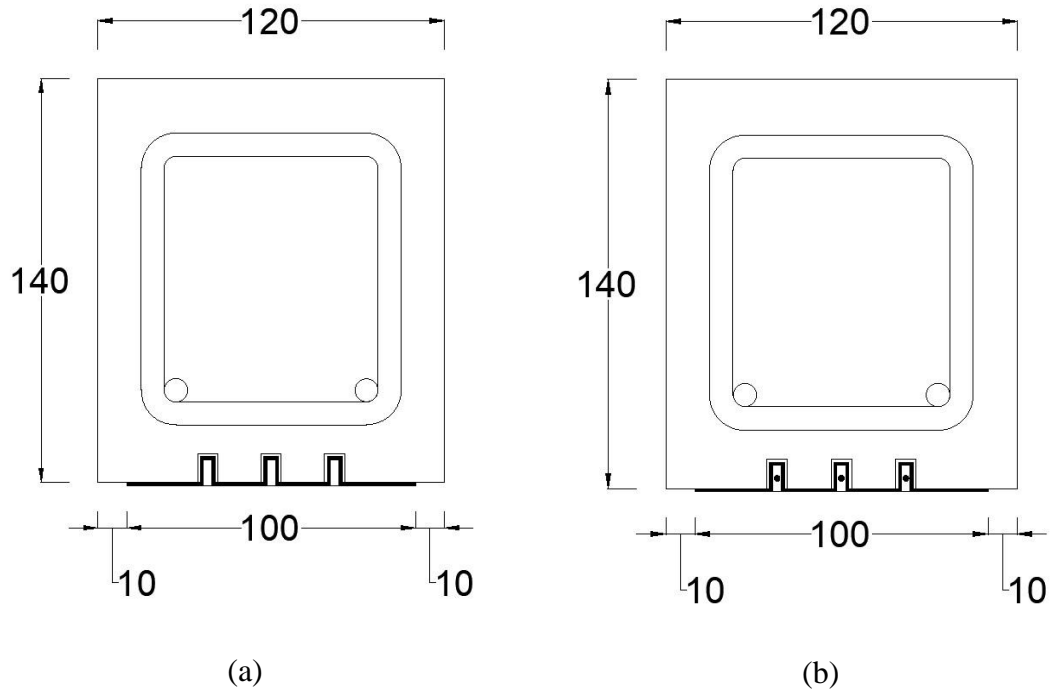


Figure 5.1 Cross-section view of strengthened beams: (a) EBRIG, (b) Combined EBRIG-NSM rods.

5.1 Effect of Groove Depth on EBRIG Strengthened RC Beams with Various Number of CFRP layers

The ultimate loads and failure modes of EBRIG beams strengthened with one, two, and three CFRP layers and varying groove depths ranging from 6 to 18 mm are shown in Table 5.1. All models had three grooves.

Table 5.1 Ultimate load capacity of beams strengthened by different layers of EBRIG with varying groove depths

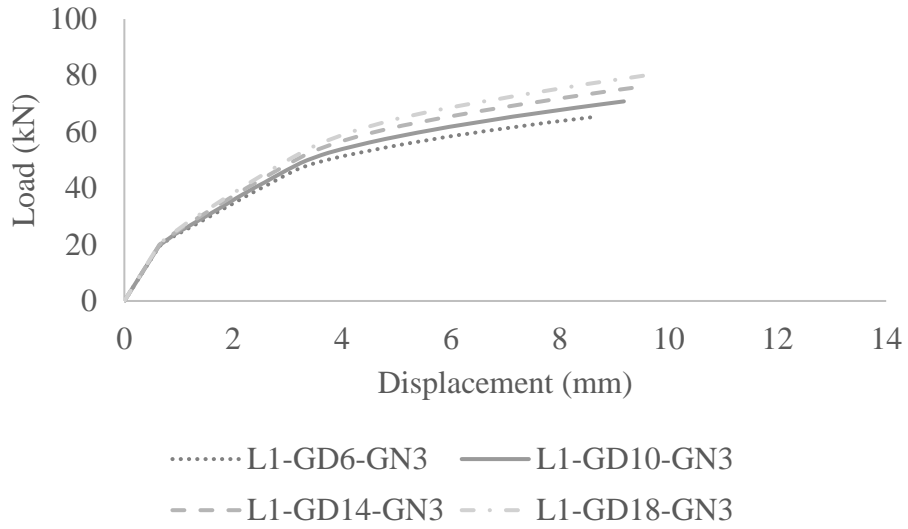
Beam ID	Number of CFRP layers	Groove depths (mm)	Ultimate load capacity (kN)	Load increase relative to CB (%)	Failure mode
CB			36.7		Yielding of steel
1L-GD6-GN3	1	6	65.2	77.41	FRP Rupture
1L-GD10-GN3	1	10	70.8	92.65	FRP Rupture
1L-GD14-GN3	1	14	75.8	106.26	FRP Rupture
1L-GD18-GN3	1	18	80.6	119.32	FRP Rupture
2L-GD6-GN3	2	6	94.0	155.65	Concrete cover separation
2L-GD10-GN3	2	10	95.6	160.19	Concrete cover separation
2L-GD14-GN3	2	14	97.6	165.58	Concrete cover separation
2L-GD18-GN3	2	18	99.9	171.81	Concrete cover separation
3L-GD6-GN3	3	6	99.7	171.24	Concrete cover separation
3L-GD10-GN3	3	10	101.4	175.99	Concrete cover separation
3L-GD14-GN3	3	14	102.8	179.73	Concrete cover separation
3L-GD18-GN3	3	18	103.6	181.90	Concrete cover separation

The rupture of FRP was the mode of failure in the beams strengthened with a single layer, whereas the beams with double and triple layers failed by concrete cover separation. The ultimate load capacity of the beams improved with the increase in the groove depth. The ultimate loads of EBRIG strengthened beams with 18 mm groove depth and a single, double, and triple layer of FRP sheets were 23.6, 6.3, and 3.9% more than the beams with 6 mm groove depth and corresponding number of CFRP layers. It can be concluded that the groove depth contribution was more prominent in EBRIG strengthened beams with one FRP layer.

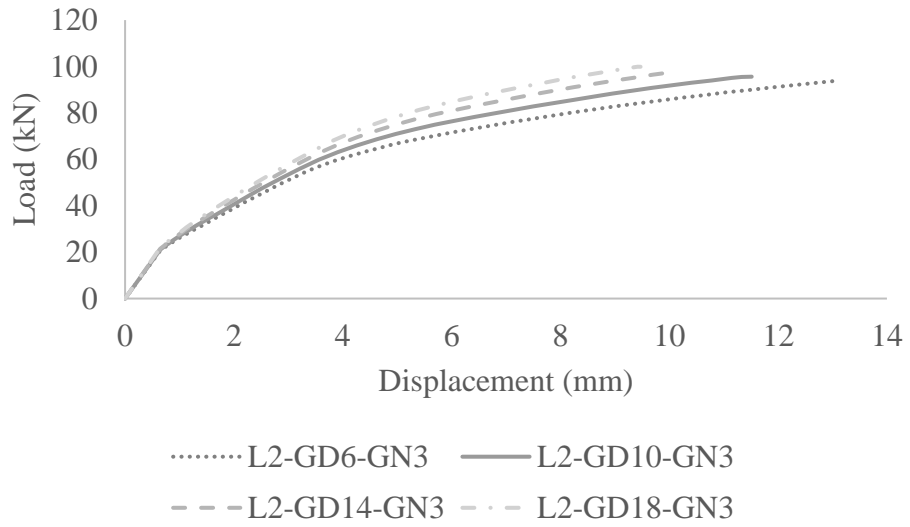
The maximum load increases relative to the control beam observed in single, double, and triple-layered EBRIG strengthened beams were 119.3, 171.8, and 181.9%,

respectively. The load capacity increases considerably for all depths when going from one layer to two layers. However, the difference of ultimate load is more negligible between double and triple layers of FRP. The failure mode of double layered EBRIG was the concrete cover separation which was controlled by the tensile strength of concrete. Therefore, the addition of FRP layer did not contribute significantly in increasing the load capacity of the strengthened beams.

The load versus displacement curves of EBRIG strengthened beams with different groove depths, and FRP layers are shown in Fig. 5.2. The stiffness of the beams increased with the increase in groove depths after the formation of initial cracks. The ultimate mid-span displacements of single-layered EBRIG strengthened beams increased with the groove depths. The trend was just the opposite for EBRIG with two or three layers of CFRP. The variation in the trend can be attributed to the difference in the mode of failure.

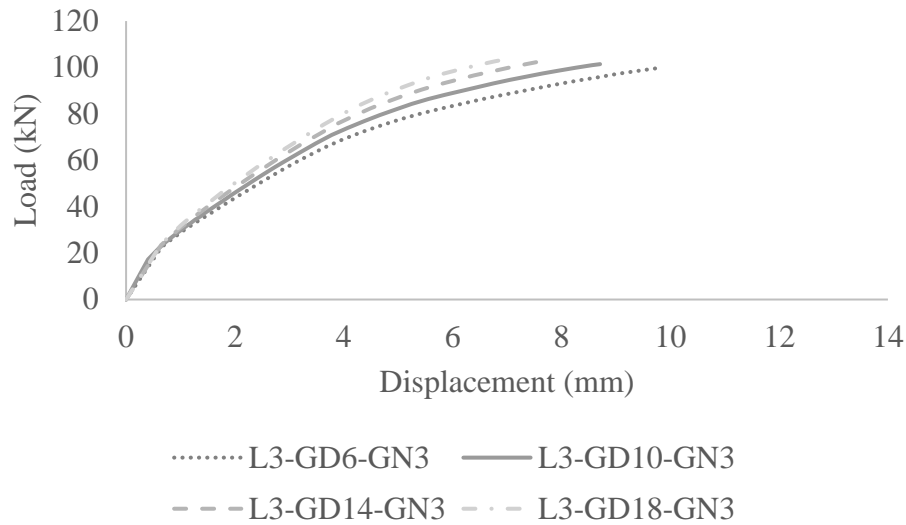


(a)



(b)

Figure 5-2 (a and b)



(c)

Figure 5.2 (c) Load versus displacement curve of EBRIG strengthened beams with different groove depths for (a) single CFRP layer, (b) double CFRP layer, and (c) triple CFRP layer.

5.2 Effect of Number of Grooves on EBRIG Strengthened RC Beams with Various Number of CFRP layers

The ultimate loads and failure modes of EBRIG beams strengthened with one, two, and three CFRP layers and varying number of grooves ranging from 1 to 5 are shown in Table 5.2. The rupture of FRP was the mode of failure in the beams strengthened with a single layer, whereas the beams with double and triple layers failed by concrete cover separation. The maximum load increases relative to the control beam observed in single,

double, and triple-layered EBRIG strengthened beams were 119.3, 175.7, and 182.2%, respectively.

Table 5.2 Ultimate Load Capacity of Beams Strengthened by Various Layers of EBRIG and Groove Numbers

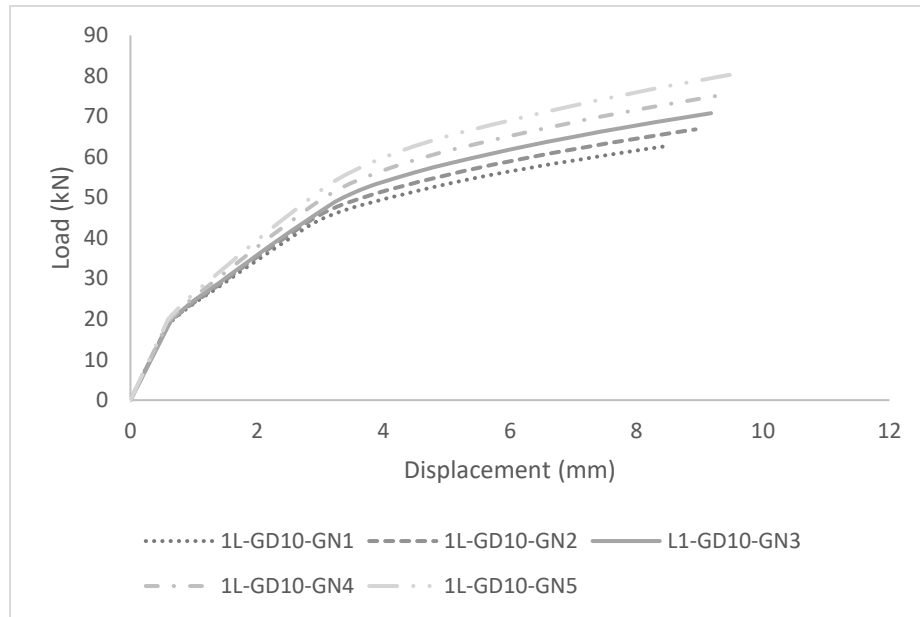
Beam ID	Number of FRP layers	Number of grooves	Ultimate load capacity (kN)	Load increase relative to control beam (CB) (%)	Failure mode
CB			36.7		
L1-GD10-GN1	1	1	62.8	70.8	FRPR
L1-GD10-GN2	1	2	66.8	81.7	FRPR
L1-GD10-GN3	1	3	70.8	92.6	FRPR
L1-GD10-GN4	1	4	75.5	105.4	FRPR
L1-GD10-GN5	1	5	80.6	119.3	FRPR
L2-GD10-GN1	2	1	87.9	139.2	CCS
L2-GD10-GN2	2	2	92.6	152.0	CCS
L2-GD10-GN3	2	3	95.6	160.2	CCS
L2-GD10-GN4	2	4	98.9	169.1	CCS
L2-GD10-GN5	2	5	101.3	175.7	CCS
L3-GD10-GN1	3	1	96.1	161.5	CCS
L3-GD10-GN2	3	2	99.3	170.2	CCS
L3-GD10-GN3	3	3	101.4	176.0	CCS
L3-GD10-GN4	3	4	103.5	181.6	CCS
L3-GD10-GN5	3	5	103.7	182.2	CCS

FRPR: FRP rupture; CCS: Concrete cover separation

The ultimate load capacity of the beams improved with the increase in the number of grooves. The ultimate loads of EBRIG strengthened beams with 5 grooves and a single, double, or triple layer of FRP sheets were 28.3, 15.2, and 7.9% more than the beam with a single groove and corresponding number of CFRP layers. The enhancement in the load capacity was due to additional FRP materials with an increase in groove number. It was

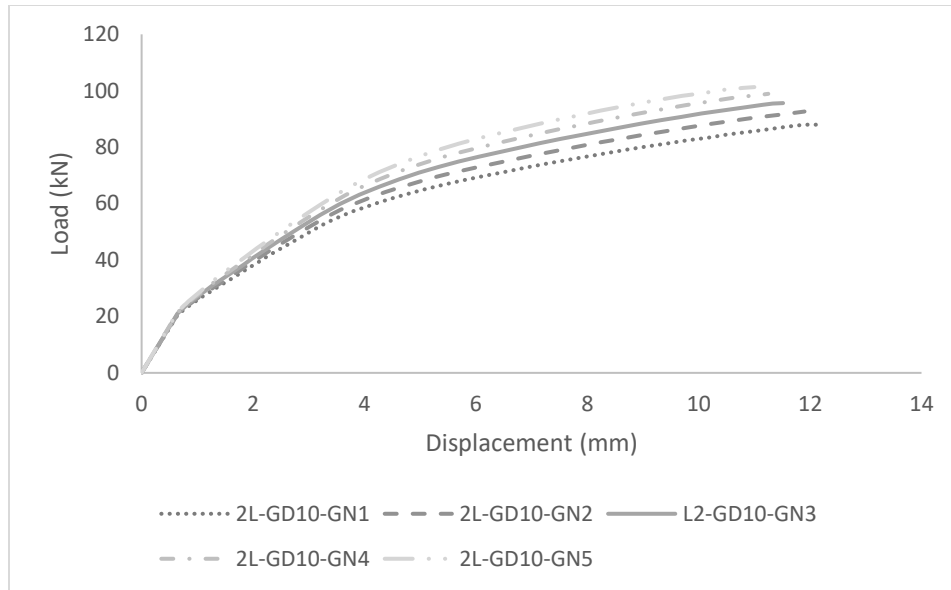
observed that the effect of groove was more prominent in EBRIG strengthened beams with one FRP layer. As the strengthened beams with double and triple layers of FRP failed by concrete cover separation, the additional FRP materials provided by the increase in groove numbers did not result in significant improvement in the load capacity.

The load versus displacement curves of beams strengthened with various number of grooves for single, double, and triple-layered EBRIG are shown in Fig. 5.3. The ultimate mid-span deflection increased with the number of grooves in single-layered EBRIG, while the trend was just the opposite in double and triple-layered EBRIG. Similar observations were made with the groove depth increase.

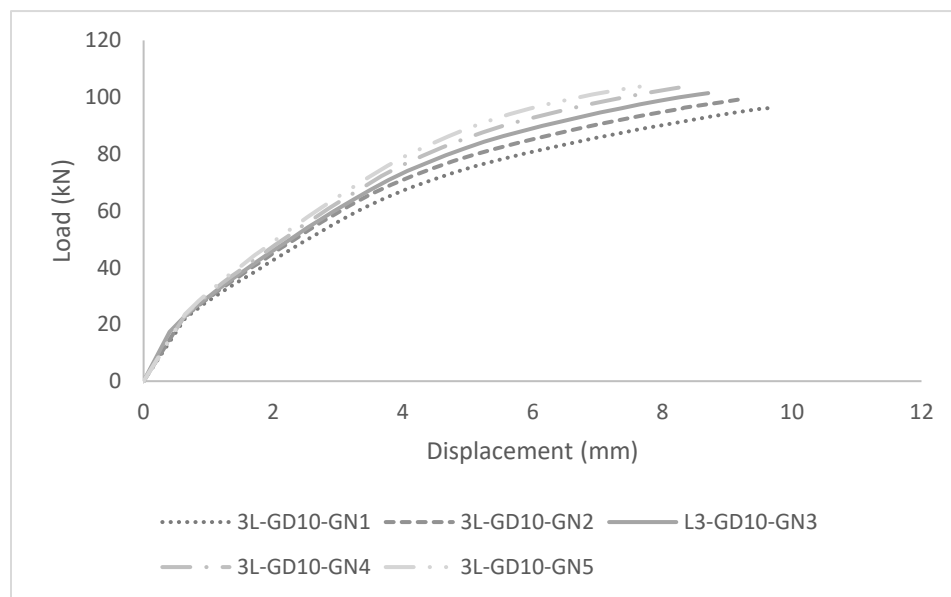


(a)

Figure 5-3 (a)



(b)



(c)

Figure 5.3(b and c) Load versus displacement curve of CBRIG strengthened beams with various groove numbers for (a) single CFRP layer, (b) double CFRP layer, and (c) triple CFRP layer.

5.3 Combined EBRIG and NSM Strengthening of RC Beams

In combined EBRIG and NSM strengthening of RC beams, the FRP sheets are applied inside entire grooves with subsequent insertion of FRP rods in the grooves as NSM reinforcement for further strengthening purpose. CFRP rods of different diameters varying from 1 mm to 4 mm were installed at the centroid of the grooves. The different sizes of FRP rods were selected from product datasheet of ACP Composites (ACP Composites, 2014). The ultimate load capacity and failure modes of the strengthened beams are shown in Table 5.3.

Table 5.3 Ultimate Load Capacity of Beams Strengthened by Combined EBRIG-NSM Rods

Beam ID	Number of CFRP layers	NSM FRP rod diameter (mm)	Ultimate load capacity (kN)	Load increase relative to control beam (CB) (%)	Failure mode
CB			36.7		
1L-GD10-GN3	1	0	70.8	92.9	FRPR
1L-GD10-GN3- ϕ 1	1	1	72.8	98.4	FRPR
1L-GD10-GN3- ϕ 2	1	2	78.5	114.0	FRPR
1L-GD10-GN3- ϕ 3	1	3	87.0	137.0	FRPR
1L-GD10-GN3- ϕ 4	1	4	92.6	152.4	CCS
2L-GD10-GN3	2	0	95.6	160.5	CCS
2L-GD10-GN3- ϕ 1	2	1	95.9	161.4	CCS
2L-GD10-GN3- ϕ 2	2	2	96.1	162.0	CCS
2L-GD10-GN3- ϕ 3	2	3	95.8	161.0	CCS
2L-GD10-GN3- ϕ 4	2	4	93.9	155.7	CCS
3L-GD10-GN3	3	0	101.4	176.4	CCS
3L-GD10-GN3- ϕ 1	3	1	101.1	175.6	CCS
3L-GD10-GN3- ϕ 2	3	2	100.1	172.7	CCS
3L-GD10-GN3- ϕ 3	3	3	97.9	166.9	CCS
3L-GD10-GN3- ϕ 4	3	4	95.0	158.9	CCS

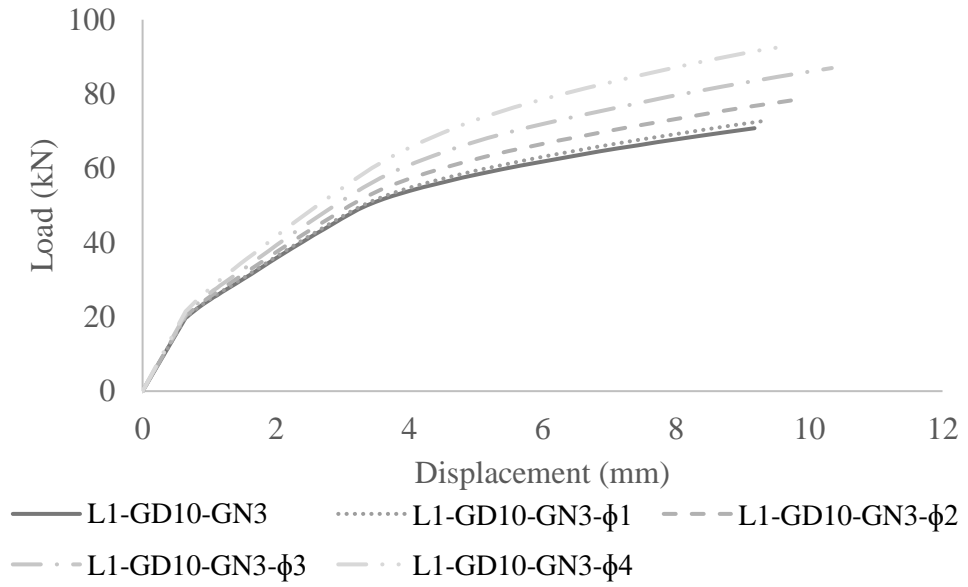
FRPR: FRP Rupture; CCS: Concrete Cover separation

All the beams with combined single layered EBRIG and NSM failed by the rupture of CFRP fabric, except the one with 4 mm NSM FRP bar, which failed by concrete cover separation. The beams with more FRP layers combined with NSM rods failed by concrete cover separation.

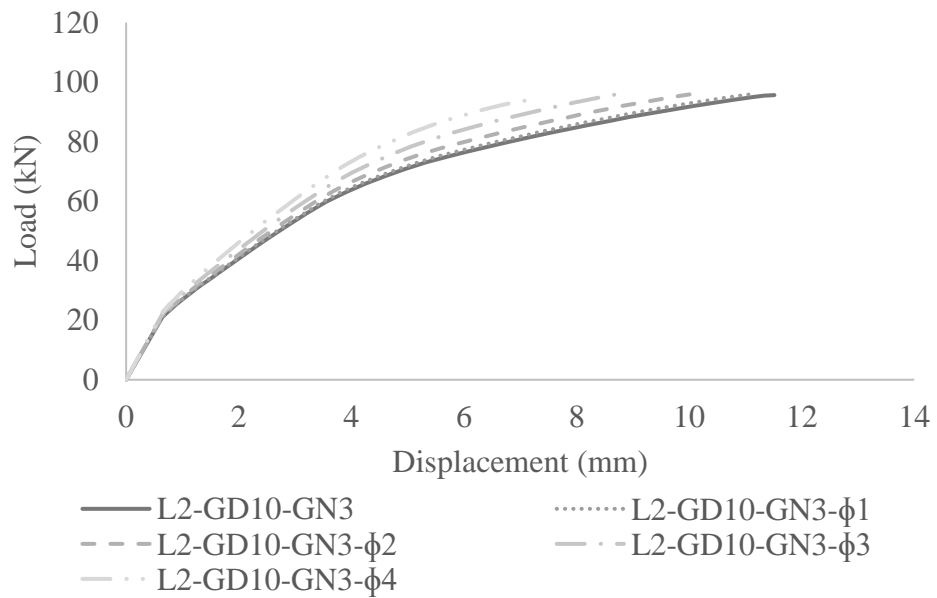
For beams with a single layer of EBRIG, the load capacity enhanced with the increase in diameter of NSM FRP rods. The maximum load in beam strengthened by single layer

EBRIG combined with 4 mm NSM rod was 92.2 kN, which was 30.7% increase relative to the corresponding EBRIG strengthened beam without NSM rod. Once the number of FRP layers was increased to two and three in combined EBRIG-NSM rod strengthened beams, there was no further improvement in the load capacity as compared to EBRIG counterpart beams. When the failure mode of the strengthened beam shifted to concrete cover separation, further increase in CFRP ratio by NSM rods did not enhance the load capacity of the strengthened beams. Rather, the increased stiffness expedites the tensile stress generation at the substrate concrete and cause earlier debonding, decreasing the load capacity. Similar results were obtained by (Godat et al., 2020; Metwally, 2014), when thickness or layers of FRP materials were further increased in strengthened beams which previously failed by debonding. For the beams strengthened by combined EBRIG-NSM rod with same rod size, the load capacity improved with addition of number of CFRP layers.

The load versus displacement curves of beams strengthened with the different NSM sizes are shown in Fig. 5.4. The ultimate mid-span displacement in combined single layered EBRIG- NSM rod strengthening increased when the size of the rod was increased from 0 mm to 3 mm. However, when the rod diameter was 4 mm, the ultimate mid-span displacement reduced. The change in the trend can be attributed to transition of failure mode from FRP rupture to concrete cover separation. The ultimate mid-span displacements decreased consistently with an increase in NSM bar diameter for the beams strengthened with combined EBRIG-NSM rod with two or three FRP layers.

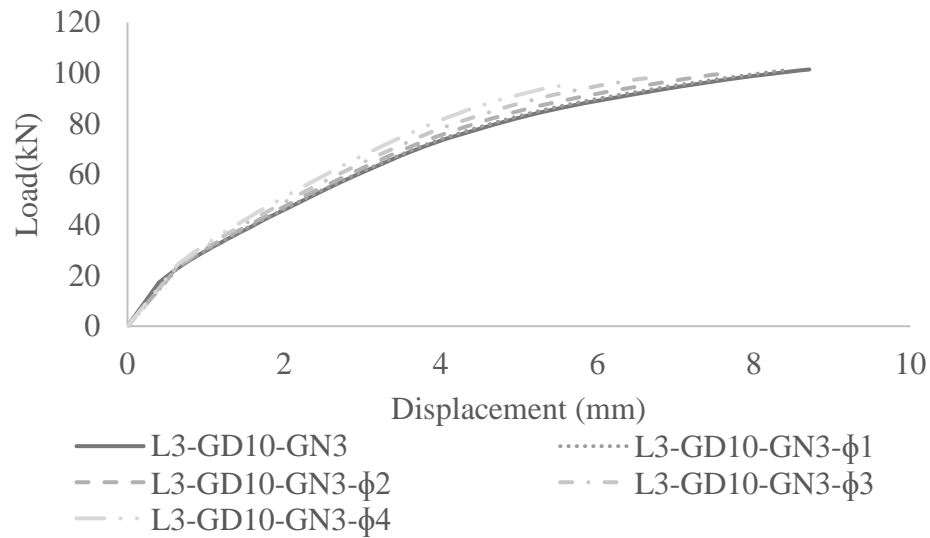


(a)



(b)

Figure 5-4 (a and b)



(c)

Figure 5.4 (c) Load versus displacement curve of beams strengthened by combined EBRIG-NSM rods with various rod diameters and (a) single CFRP layer, (b) double CFRP layer, and (c) triple CFRP layer.

5.4 Effect of Different Groove Depths on Combined EBRIG-NSM Rod Strengthened Beams

Next, the role of groove depth was studied for combined EBRIG-NSM rod strengthened beams. The beams externally bonded with the single CFRP layer and various

size NSM rods in grooves were selected. NSM FRP rods of 2, 3, and 4 mm in diameter were installed at the centroid of three grooves of 7 mm width spaced at 15 mm and various groove depths ranging from 6 to 18 mm. The ultimate loads and failure modes of these strengthened beams are shown in Table 5.4.

Table 5.4 Ultimate Load Capacity of Combined EBRIG-NSM Rods Strengthened Beams with Various Groove Depths

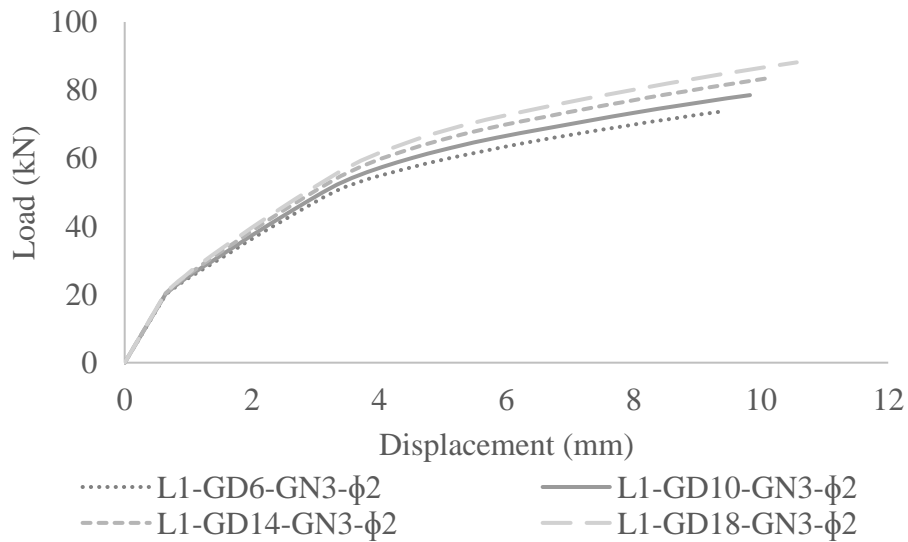
Beam ID	NSM FRP rod diameter (mm)	Groove depths (mm)	Ultimate load capacity (kN)	Load increase relative to control beam (CB) (%)	Failure mode
CB			36.7		
1L-GD6-GN3- ϕ 2	2	6	73.3	99.7	FRPR
1L-GD10-GN3- ϕ 2	2	10	78.5	114.0	FRPR
1L-GD14-GN3- ϕ 2	2	14	83.5	127.5	FRPR
1L-GD18-GN3- ϕ 2	2	18	88.1	140.2	FRPR
1L-GD6-GN3- ϕ 3	3	6	82.1	123.8	FRPR
1L-GD10-GN3- ϕ 3	3	10	87.0	137.0	FRPR
1L-GD14-GN3- ϕ 3	3	14	91.3	148.9	FRPR
1L-GD18-GN3- ϕ 3	3	18	95.3	159.7	FRPR
1L-GD6-GN3- ϕ 4	4	6	90.6	146.9	CCS
1L-GD10-GN3- ϕ 4	4	10	92.6	152.4	CCS
1L-GD14-GN3- ϕ 4	4	14	94.6	157.8	CCS
1L-GD18-GN3- ϕ 4	4	18	96.5	162.9	CCS

FRPR: FRP Rupture; CCS: Concrete Cover Separation

The rupture of FRP was the mode of failure in the beams strengthened with 2 and 3 mm NSM rod, whereas the beams with 4 mm rod failed by the concrete cover separation. When the failure mode changed from FRP rupture to concrete cover separation, the groove depth effect was minimal. However, in the case of FRP rupture failure, the higher groove depth

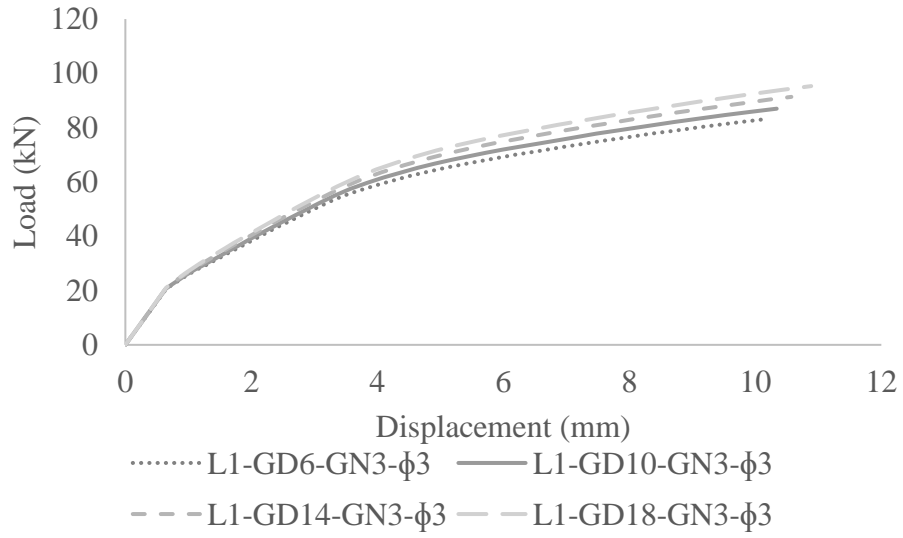
contributed to ultimate load capacity increase of the beam. The ultimate load capacity of the beams improved with the increase in the groove depths. The ultimate loads on the strengthened beam with 18 mm groove depth and 2, 3, and 4 mm CFRP NSM rods were 20.1, 16.1, and 6.5% more than the beam with 6 mm groove depth and the corresponding size of NSM rods. The enhancement in the load capacity was due to additional FRP materials with an increase in groove depth.

The load versus displacement curves of strengthened beams with single-layered EBRIG-NSM rods and various groove depths for 2, 3, and 4mm diameter-rods are shown in Fig. 5.5. Similar to the previous observations, when the failure mode was the FRP rupture, the ultimate displacements increased with the FRP reinforcement attributed to the increased groove depths. When the failure mode was the concrete cover separation, the opposite was true.

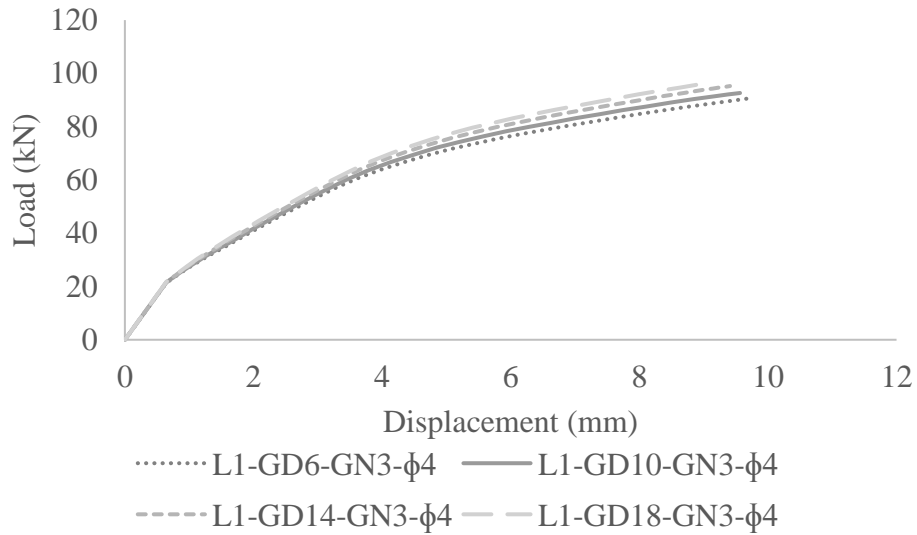


(a)

Figure 5-5 (a)



(b)



(c)

Figure 5.5 (b and c) Load versus displacement curve of beams strengthened by combined EBRIG-NSM rods with single layer of FRP and various groove depths with (a) 2 mm NSM rod, (b) 3 mm NSM rod, and (c) 4 mm NSM rod.

5.5 Effect of Various Number of Grooves on Combined EBRIG-NSM Rod Strengthened Beams

To investigate the role of groove depth on combined EBRIG-NSM rod strengthened beams, the beams externally bonded with the single CFRP layer and various size NSM rods in grooves were selected. NSM FRP rods of 2, 3, and 4 mm in diameter were installed at the centroid of 1 to 5 grooves of 7 mm width, and 10 mm height spaced at 15 mm. The ultimate loads and failure modes of these strengthened beams are shown in Table 5.5.

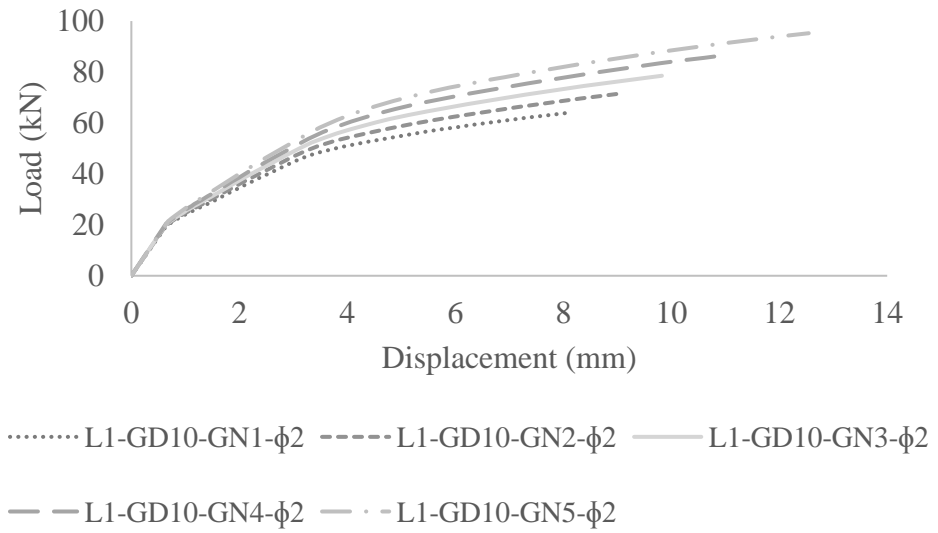
Table 5.5 Ultimate Load Capacity of Combined EBRIG-NSM Rods Strengthened Beams with Various Groove Numbers

Beam ID	NSM FRP rod diameter (mm)	Number of grooves	Ultimate load capacity (kN)	Load increase relative to control beam (CB) (%)	Failure mode
CB			36.7		
1L-GD10-GN1- ϕ 2	2	1	63.8	74.0	FRPR
1L-GD10-GN2- ϕ 2	2	2	71.7	95.3	FRPR
1L-GD10-GN3- ϕ 2	2	3	78.5	114.0	FRPR
1L-GD10-GN4- ϕ 2	2	4	86.7	136.2	FRPR
1L-GD10-GN5- ϕ 2	2	5	95.2	159.4	FRPR
1L-GD10-GN1- ϕ 3	3	1	69.7	90.0	FRPR
1L-GD10-GN2- ϕ 3	3	2	78.5	113.9	FRPR
1L-GD10-GN3- ϕ 3	3	3	87.0	137.0	FRPR
1L-GD10-GN4- ϕ 3	3	4	95.3	159.6	FRPR
1L-GD10-GN5- ϕ 3	3	5	99.9	172.2	CCS
1L-GD10-GN1- ϕ 4	4	1	73.6	100.5	FRPR
1L-GD10-GN2- ϕ 4	4	2	84.0	129.0	CCS
1L-GD10-GN3- ϕ 4	4	3	92.6	152.4	CCS
1L-GD10-GN4- ϕ 4	4	4	97.9	166.9	CCS
1L-GD10-GN5- ϕ 4	4	5	100.4	173.7	CCS

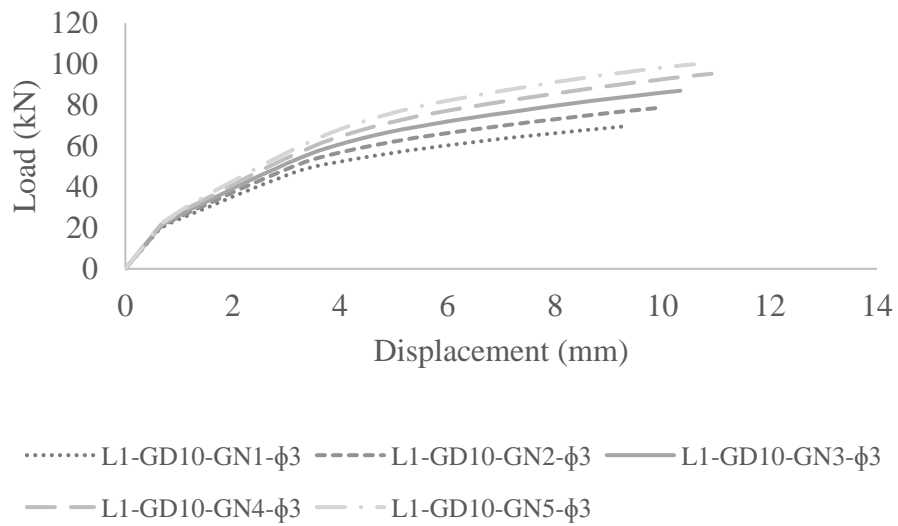
Failure mode of all the beams with 2 mm, and 3 mm NSM rods failed by FRP rupture, except the one with 3 mm NSM rods in five grooves, which failed by concrete cover separation. Beam with 4 mm NSM rods in single groove failed by FRP rupture, while the beams with more grooves failed by concrete cover separation.

The ultimate load capacity of the beams improved with the increase in the groove numbers. The ultimate load of the strengthened beam with 2, 3, and 4 mm CFRP NSM rod in 5 grooves were 49.2, 43.3, and 36.41% more than the beam with a single groove and corresponding size of NSM rods. The enhancement in the load capacity was due to additional FRP reinforcement with an increase in groove numbers. As compared to the control beam (CB), the load increases and the failure mode in strengthened beam with 3 mm rod 5 grooves and the beam with 4 mm NSM rod and 5 grooves were almost the same. This observation indicates the 4 mm NSM diameter bars combined with 5 grooves is the optimal configuration in strengthening of the beams considered in the present study.

The load versus displacement curves of strengthened beams with single-layered EBRIG-NSM rods and various groove numbers for 2, 3, and 4 mm diameter-rods are shown in Fig. 5.6. Similar to the previous observations, when the failure mode was the FRP rupture, the ultimate displacements increased with the FRP reinforcement attributed to the additional grooves. When the failure mode was the concrete cover separation, the opposite was true.

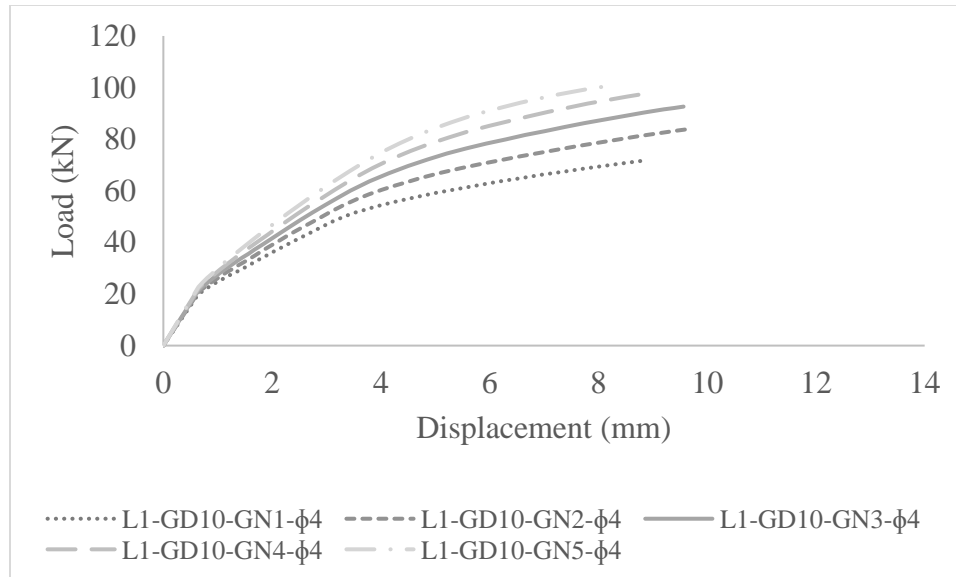


(a)



(b)

Figure 5-6 (a and b)



(c)

Figure 5.6 Load versus displacement curve of combined EBRIG-NSM rod strengthened beams with single layer of FRP and various number of grooves with (a) 2 mm NSM rods, (b) 3 mm NSM rods, and (c) 4 mm NSM rods.

Chapter 6

Conclusions

In this research, finite element models of RC beams strengthened by EBRIG technique were validated through an experimental study in the literature. The validated FE beam models were then used to perform parametric study. Further strengthening of the beams were investigated using a combination of EBRIG and NSM technique. The impact of groove depths and groove numbers was also studied for the beams strengthened by EBRIG and EBRIG-NSM bars. The following conclusions can be drawn from the current study:

1. The load versus displacement curves of the FE validated models (CB, S1, S2 and S3) were in good agreement with the experimental results, with less than 7% and 9% discrepancies in ultimate load and midspan displacement, respectively. The failure modes of the FE beam models also conformed with the experimental beams.
2. EBRIG technique was an efficient method for the flexural strengthening of RC beams. The maximum load capacity improvement achieved in EBRIG strengthened beam was 182.2% relative to the control beam, when triple layer of FRP and five grooves were provided.
3. Combining EBRIG method with NSM technique was effective to enhance the load capacity of the beam with the single layered FRP. The ultimate load in combined EBRIG-NSM rod strengthened beam with single layer of FRP and 4 mm NSM bar in

three grooves increased by 30.7% relative to corresponding EBRIG strengthened beam without NSM rod. Improvement in the load capacity was not observed in the combined EBRIG-NSM rod strengthened beams with two or three layers of FRP. As compared to the control beam, the highest load capacity improvement achieved in combined EBRIG-NSM rod strengthened beam was 173.7%, when single layer of CFRP was provided with 4 mm NSM rods in five grooves.

4. In the case of EBRIG and combined EBRIG-NSM rod strengthened beams with three grooves, the load capacity enhanced with the increase in the groove depth. As compared to the EBRIG strengthened beams with double and triple layers of FRP, the ultimate load of beam reinforced with a single layer showed the highest increment of 23.6% when the groove depth changed from 6 to 18 mm. The peak load in combined EBRIG-NSM rod strengthened beam with single layer FRP, and 2 mm NSM rod increased by 20.1% when the groove depth varied from 6 to 18 mm.
5. For EBRIG as well as combined EBRIG-NSM rod strengthened beams, the load capacity improved with additional grooves. When number of grooves changed from 1 to 5, the ultimate load of EBRIG and combined EBRIG-NSM rod (2 mm) strengthened beams enhanced by 28.3% and 49.2%, respectively.
6. For combined EBRIG-NSM strengthened beams with single layer of FRP sheet, the load capacity improved with larger NSM rod diameter. For combined EBRIG-NSM rod strengthened beams with single layer of FRP sheet, five grooves with 3 mm NSM rods was the optimal scenario since no significant improvement was observed in the ultimate load capacity when the rod size was changed from 3 to 4 mm. The load

capacity improved with addition of number of FRP layers in the combined EBRIG-NSM rod strengthened beams with the same NSM reinforcement size.

7. In the case of EBRIG strengthened beams, the groove depths and groove numbers did not change the failure mode. Similarly, in the case of combined EBRIG-NSM strengthened beams, the failure mode was unaltered by the change in groove depths. However, with the increase in number of grooves or the size of NSM rods, the failure mode shifted from the rupture of FRP sheets to concrete cover separation.
8. When the failure mode of the strengthened beams was the FRP rupture, the ultimate displacement of the beams increased with addition of FRP reinforcement. The opposite was true when the failure mode was concrete cover separation.
9. Among the several parameters considered, number of CFRP layers is the most effective parameter to affect the load capacity and the failure modes of the beams.

Chapter 7

Recommendations and Future Work

This chapter presents recommendations based on the current study and possible areas for future studies.

7.1 Recommendations

CFRP EBRIG strengthening technique is an efficient method for the flexural strengthening of concrete beams. The effectiveness of EBRIG technique can be enhanced by increasing the number of CFRP layers, depth of grooves, and the number of grooves. The number of CFRP layers is the most influential parameter in affecting the strengthening of RC beams by EBRIG. The combination of EBRIG method with NSM technique could not contribute to enhancing the load capacity of the beams relative to EBRIG strengthened beams. So, EBRIG strengthening is more effective than the combined EBRIG-NSM strengthening technique.

7.2 Future work

The validated experimental and FE beams used in the current study were scale-down models. So, to know the actual behavior of EBRIG strengthening of RC beams, investigations need to be done in the future with real-size experimental beams. After the data of real-size experimental beams become available, further study of different

parameters affecting the strengthening method can be done using numerical methods. The present study investigates the EBRIG strengthening of RC beams using CFRP sheets. EBRIG strengthening of the beams using other types of FRPs like GFRP, BFRP, and AFRP can be studied in the future.

References

- ACI318. (2019). *Building Code Requirements for Structural Concrete and Commentary*.
- ACI440.2R. (2017). Guide for the Design and Construction of Externally Bonded FRP Systems for Strengthening Concrete Structures
- ACP Composites. (2014). Product data sheet.
- Amiri, S., & Talaeitaba, S. B. (2020). Punching shear strengthening of flat slabs with EBROG and EBRIG–FRP strips. Structures,
- ANSYS. (2020). *ANSYS Mechanical APDL 2020 R2*. ANSYS INC.
- Bangash, M. (1989). Concrete and concrete structures: Numerical modelling and applications.
- Bilotta, A., Ceroni, F., Di Ludovico, M., Nigro, E., Pecce, M., & Manfredi, G. (2011). Bond efficiency of EBR and NSM FRP systems for strengthening concrete members. *Journal of composites for construction*, 15(5), 757-772.
- Bisby, L., & Fitzwilliam, J. (2006). An introduction to FRP composites for construction. *ISIS education module, Manitoba, Canada*.
- Chansawat, K., Yim, S. C., & Miller, T. H. (2006). Nonlinear finite element analysis of a FRP-strengthened reinforced concrete bridge. *Journal of Bridge Engineering*, 11(1), 21-32.
- Chong, K. T. (2004). *Numerical modelling of time-dependent cracking and deformation of reinforced concrete structures*. University of New South Wales.

- Desayi, P., & Krishnan, S. (1964). Equation for the stress-strain curve of concrete. Journal Proceedings,
- Duthinh, D., & Starnes, M. (2004). Strength and ductility of concrete beams reinforced with carbon fiber-reinforced polymer plates and steel. *Journal of composites for construction*, 8(1), 59-69.
- Fanning, P. (2001). Nonlinear models of reinforced and post-tensioned concrete beams. *Electronic Journal of Structural Engineering*, 1(2), 111-119.
- Fardis, M. N., & Khalili, H. (1981). Concrete encased in fiberglass-reinforced plastic. Journal Proceedings,
- Godat, A., Chaallal, O., & Obaidat, Y. (2020). Non-linear finite-element investigation of the parameters affecting externally-bonded FRP flexural-strengthened RC beams. *Results in Engineering*, 8, 100168.
- Hawileh, R. A. (2012). Nonlinear finite element modeling of RC beams strengthened with NSM FRP rods. *Construction and Building Materials*, 27(1), 461-471.
- Hognestad, E., Hanson, N. W., & McHenry, D. (1955). Concrete stress distribution in ultimate strength design. Journal Proceedings,
- Jeevanantham, R., Venketaramanmurthy, V., & Rajeswari, D. (2016). Mechanical and wear characterization of basalt fiber reinforced polyurethane composites. *International Journal of Advances in Engineering & Technology*, 9, 79-83.
- Jia, M. (2003). *Finite element modeling of reinforced concrete beams strengthened with FRP composite sheets*. The University of Alabama in Huntsville.
- JSCE. (2001). Recommendations for Upgrading of Concrete Structures with Use of Continuous Fiber Sheet.

- Kachlakev, D. I., Miller, T. H., Potisuk, T., Yim, S. C., & Chansawat, K. (2001). *Finite element modeling of reinforced concrete structures strengthened with FRP laminates*.
- Katsumata, H., Kobatake, Y., & Takeda, T. (1987). 'A study on the strengthening with carbon fiber for earthquake-resistant capacity of existing reinforced concrete columns. Proc., Workshop on Repair and Retrofit of Existing Structures,
- Kaw, A. K. (2005). *Mechanics of composite materials*. CRC press.
- Kotynia, R. (2012). Bond between FRP and concrete in reinforced concrete beams strengthened with near surface mounted and externally bonded reinforcement. *Construction and Building Materials*, 32, 41-54.
- Lee, D., Cheng, L., & Yan-Gee Hui, J. (2013). Bond characteristics of various NSM FRP reinforcements in concrete. *Journal of composites for construction*, 17(1), 117-129.
- Lu, X., Ye, L., Teng, J., & Jiang, J. (2005). Meso-scale finite element model for FRP sheets/plates bonded to concrete. *Engineering structures*, 27(4), 564-575.
- Malek, A. M., Saadatmanesh, H., & Ehsani, M. R. (1998). Prediction of failure load of R/C beams strengthened with FRP plate due to stress concentration at the plate end. *ACI structural Journal*, 95, 142-152.
- Meier, U. (1987). Bridge repair with high performance composite materials. *Material und Technik*, 4, 125-128.
- Metwally, I. M. (2014). Three-dimensional finite element analysis of reinforced concrete slabs strengthened with epoxy-bonded steel plates. *Advances in concrete construction*, 2(2), 091.

- Model Code*. (2010). International Federation for Structural Concrete (fib).
- Mostofinejad, D., & Hajrasouliha, M. (2011). Experimental study on grooving detail for elimination of debonding of FRP sheets from concrete surface. In *Advances in FRP Composites in Civil Engineering* (pp. 545-547). Springer.
- Mostofinejad, D., & Kashani, A. T. (2013). Experimental study on effect of EBR and EBROG methods on debonding of FRP sheets used for shear strengthening of RC beams. *Composites part B: engineering*, 45(1), 1704-1713.
- Mostofinejad, D., & Mahmoudabadi, E. (2010). Grooving as alternative method of surface preparation to postpone debonding of FRP laminates in concrete beams. *Journal of composites for construction*, 14(6), 804-811.
- Mostofinejad, D., & Shameli, M. (2011). Performance of EBROG method under multilayer FRP sheets for flexural strengthening of concrete beams. *Procedia Engineering*, 14, 3176-3182.
- Mostofinejad, D., & Shameli, S. M. (2013). Externally bonded reinforcement in grooves (EBRIG) technique to postpone debonding of FRP sheets in strengthened concrete beams. *Construction and Building Materials*, 38, 751-758.
- Mostofinejad, D., Shameli, S. M., & Hosseini, A. (2014). EBROG and EBRIG methods for strengthening of RC beams by FRP sheets. *European journal of environmental and civil engineering*, 18(6), 652-668.
- Nanni, A., & Bradford, N. M. (1995). FRP jacketed concrete under uniaxial compression. *Construction and Building Materials*, 9(2), 115-124.

- Neale, K., Ebead, U., Abdel Baky, H., Elsayed, W., & Godat, A. (2005). Modelling of debonding phenomena in FRP-strengthened concrete beams and slabs. *International Institute for FRP in Construction*.
- Nguyen, D. M., Chan, T. K., & Cheong, H. K. (2001). Brittle failure and bond development length of CFRP-concrete beams. *Journal of composites for construction*, 5(1), 12-17.
- Oehlers, D. J. (2006). FRP plates adhesively bonded to reinforced concrete beams: Generic debonding mechanisms. *Advances in Structural Engineering*, 9(6), 737-750.
- Omran, H. Y., & El-Hacha, R. (2012). Nonlinear 3D finite element modeling of RC beams strengthened with prestressed NSM-CFRP strips. *Construction and Building Materials*, 31, 74-85.
- Pendhari, S. S., Kant, T., & Desai, Y. M. (2008). Application of polymer composites in civil construction: A general review. *Composite structures*, 84(2), 114-124.
- Seracino, R., Raizal Saifulnaz, M., & Oehlers, D. (2007). Generic debonding resistance of EB and NSM plate-to-concrete joints. *Journal of composites for construction*, 11(1), 62-70.
- Sharaky, I. A., Torres, L., Comas, J., & Barris, C. (2014). Flexural response of reinforced concrete (RC) beams strengthened with near surface mounted (NSM) fibre reinforced polymer (FRP) bars. *Composite structures*, 109, 8-22.
- Sharif, A., Al-Sulaimani, G., Basunbul, I., Baluch, M., & Ghaleb, B. (1994). Strengthening of initially loaded reinforced concrete beams using FRP plates. *Structural Journal*, 91(2), 160-168.

- Shomali, A., Mostofinejad, D., & Esfahani, M. R. (2019). Experimental study on effect of EBRIG shear strengthening method on the behavior of RC beams. *Advances in concrete construction*, 8(2), 145-154.
- Shomali, A., Mostofinejad, D., & Esfahani, M. R. (2020). Experimental and numerical investigation of shear performance of RC beams strengthened with FRP using grooving method. *Journal of Building Engineering*, 31, 101409.
- Shomali, A., Mostofinejad, D., & Esfahani, M. R. (2021). Shear strengthening of RC beams using EBRIG CFRP strips: a comparative study. *European journal of environmental and civil engineering*, 25(14), 2540-2556.
- Singh, S. B. (2015). *Analysis and design of FRP reinforced concrete structures*. McGraw Hill Professional.
- Tamuzs, V., Tepfers, R., Zile, E., & Valdmanis, V. (2007). Stability of round concrete columns confined by composite wrappings. *Mechanics of Composite Materials*, 43(5), 445-452.
- Tavárez, F. A. (2001). *Simulation of behavior of composite grid reinforced concrete beams using explicit finite element methods*. University of Wisconsin--Madison.
- Thorenfeldt, E. (1987). Mechanical properties of high-strength concrete and applications in design. Symposium Proceedings, Utilization of High-Strength Concrete, Norway, 1987,
- Todeschini, C. E., Bianchini, A. C., & Kesler, C. E. (1964). Behavior of concrete columns reinforced with high strength steels. Journal Proceedings,
- USDOT. (2007). *Users Manual for LS-DYNA Concrete Material Model 159*.

Willam, K. J. (1975). Constitutive model for the triaxial behaviour of concrete. *Proc. Intl. Assoc. Bridge Structl. Engrs*, 19, 1-30.

Wolanski, A. J. (2004). *Flexural behavior of reinforced and prestressed concrete beams using finite element analysis*.

Appendix A

ANSYS APDL Code of RC Control Beam (CB)

! units [Pa, N, m]

FINISH

/CLEAR,,

/PREP7

!Volume block of concrete

Block,0,60/1000,0,140/1000,0,1000/1000

/VIEW,1,1,1,1

/ANG,1

/REP,FAST

wpro,,-90,

wpoff,0,0,32/1000

VSBW, ALL

wpoff,0,0,84/1000

VSBW, ALL

wpro,,, 90

wpoff,0,0, 19/1000

VSBW, ALL

WPCSYS,-1,0

WPSTYLE,,,,,,,,,0

ASEL,S,LOC,Z,

AGEN,2,ALL, , , , 435/1000, ,0

ASEL,S,LOC,Z,

AGEN,2,ALL, , , , 465/1000, ,0

ASEL,S,LOC,Z,

AGEN,2,ALL, , , , 450/1000, ,0

ASEL,S,LOC,Z,

AGEN,2,ALL, , , , 550/1000, ,0

ASEL,S,LOC,Z,

AGEN,2,ALL, , , , 565/1000, ,0

ASEL,S,LOC,Z,

AGEN,2,ALL, , , , 535/1000, ,0

ASEL,S,LOC,Z,

AGEN,2,ALL, , , ,35/1000, ,0

ASEL,S,LOC,Z,

AGEN,2,ALL, , , ,65/1000, ,0

ASEL,S,LOC,Z,

AGEN,2,ALL, , , ,50/1000, ,0

ASEL,S,LOC,Z,

AGEN,2,ALL, , , ,950/1000, ,0

ASEL,S,LOC,Z,

AGEN,2,ALL, , , ,935/1000, ,0

ASEL,S,LOC,Z,

AGEN,2,ALL, , , ,965/1000, ,0

ASEL,S,LOC,Z,

AGEN,20,ALL, , , ,50, ,0

ALLSEL,

VSBA,ALL,ALL

!Make component of concrete volume

VSEL,S,LOC,Y,0,140/1000

CM,CONCRETEVOLUME,VOLU

!Create volume blocks of steel plates

BLOCK,0,60/1000,140/1000,160/1000,435/1000,465/1000

BLOCK,0,60,140/1000,160/1000,535/1000,565/1000

BLOCK,0,60,0,-20,35/1000,65/1000

BLOCK,0,60/1000,0,-20/1000,35/1000,65/1000

!Divide the volumes at the locations of discontinuity

VSEL,S,LOC,Y,150

wpoff,0,0, 450/1000

VSBW, ALL

wpoff,0,0, 100/1000

VSBW, ALL

wpro,,, 90

wpoff,0,0, 19/1000

VSBW, ALL

WPCSYS,-1,0

WPSTYLE,,,,,,,,,0

VSEL,S,LOC,Y,150/1000

CM,LOADINGPLATE,VOLU

VSEL,S,LOC,Y,-10/1000

wpoff,0,0, 50/1000

VSBW, ALL

wpoff,0,0, 900/1000

VSBW, ALL

wpro,,, 90

wpoff,0,0, 19/1000

VSBW, ALL

WPCSYS,-1,0

WPSTYLE,,,,,,,,,0

VSEL,S,LOC,Y,-10

CM,SUPPORTPLATE,VOLU

!Select component of lines at the location of longitudinal bar

LSEL,S,LOC,Y,32/1000

LSEL,R,LOC,X,19/1000

CM,LON,LINE

CMSEL,S,LON

!Make component of lines at location of stirrups

LSEL,S,LOC,Y,74/1000

LSEL,R,LOC,X,19/1000

LSEL,U,LOC,Z,

LSEL,U,LOC,Z,435/1000

LSEL,U,LOC,Z,465/1000

LSEL,U,LOC,Z,535/1000

LSEL,U,LOC,Z,565/1000

LSEL,U,LOC,Z,35/1000

LSEL,U,LOC,Z,65/1000

LSEL,U,LOC,Z,935/1000

LSEL,U,LOC,Z,965/1000

LSEL,U,LOC,Z,1000/1000

CM,SV,LINE

LSEL,S,LOC,Y,32/1000

LSEL,R,LOC,X,39.5/1000

LSEL,U,LOC,Z,

LSEL,U,LOC,Z,435/1000

LSEL,U,LOC,Z,465/1000

LSEL,U,LOC,Z,535/1000

LSEL,U,LOC,Z,565/1000

LSEL,U,LOC,Z,35/1000

LSEL,U,LOC,Z,65/1000

LSEL,U,LOC,Z,935/1000

LSEL,U,LOC,Z,965/1000

LSEL,U,LOC,Z,1000/1000

CM,SB,LINE

LSEL,S,LOC,Y,116/1000

LSEL,R,LOC,X,39.5/1000

LSEL,U,LOC,Z,

LSEL,U,LOC,Z,435/1000

LSEL,U,LOC,Z,465/1000

LSEL,U,LOC,Z,535/1000

LSEL,U,LOC,Z,565/1000

LSEL,U,LOC,Z,35/1000

LSEL,U,LOC,Z,65/1000

LSEL,U,LOC,Z,935/1000

LSEL,U,LOC,Z,965/1000

LSEL,U,LOC,Z,1000/1000

CM,ST,LINE

CMGRP,Stirrups,SB,ST,SV

CMSEL,S,Stirrups

!Concrete material properties

fuc = 33 E6 ! concrete cylinder strength

nu = 0.2

Ec = 27000 E6

fut =0.6*sqrt(fuc)

Oshear=0.2

Cshear=0.9

Cracking=fut

Crushing=-1

TCrackFactor=0.6

MPTEMP,,,,,,,,

MPTEMP,1,0

MP,EX,1,Ec

MP,NUXY,1,nu

TB,MISO,1,1,8,0

TBTEMP,0

TBPT,,0.00036667,9.90

TBPT,,0.000667,16.754

TBPT,,0.000967,22.57

TBPT,,0.001267,26.961

TBPT,,0.001567,29.984

TBPT,,0.001867,31.835

TBPT,,0.002167,32.761

TBPT,,0.002444,33

TB,CONC,1,1,9,

TBTEMP,0

TBDATA,,Oshear,Cshear,Cracking,Crushing,,

TBDATA,,,,TCrackFactor,,

!Meshing of concrete

CMSEL,S,CONCRETEVOLUME

ASLV

LSLA

LESIZE,ALL,20/1000

ET,1,SOLID65

KEYOPT,1,1,1

KEYOPT,1,7,1

KEYOPT,1,8,1

MAT,1

VMESH,CONCRETEVOLUME

!Steel rebar material properties

MP,EX,2,200000E6

MP,NUXY,2,0.3

TB,BKIN,2

TBTEMP,0

TBDATA,1,530E6,200,,,

!Define section of steel rebar

SECTYPE,4,LINK, ,Rebar8mm

```
SECDATA,50/E6,  
  
SECCONTROL,0,0  
  
!Mesh steel rebar elements  
  
ET,4,180  
  
TYPE,4  
  
MAT,2  
  
SECNUM,4  
  
TSHAP, LINE  
  
LMESH,LON  
  
LMESH,Stirrups  
  
! Material property of steel plate  
  
MP,EX,3,200000E6  
  
MP,NUXY,3,0.3  
  
!Meshing of steel plates  
  
CMSEL,S,LOADINGPLATE,VOLU  
  
CMSEL,A,SUPPORTPLATE,VOLU  
  
ASLV  
  
LSLA
```

```
LESIZE,ALL,20/1000

ET,3,185

TYPE, 3

MAT, 3

REAL, 3

ESYS, 0

SECNUM, ,

MSHAPE,0,3d

MSHKEY,1

CMSEL,S,LOADINGPLATE,VOLU

CMSEL,A,SUPPORTPLATE,VOLU

VMESH,LOADINGPLATE

VMESH,SUPPORTPLATE

NSEL,S,LOC,Y,140/1000

NSEL,A,LOC,Y,0

NUMMRG,NODE, , , ,LOW

/Solution
```

! Hinge Support

NSEL,S,LOC,Y,-20/1000

NSEL,R,LOC,Z, 50/1000,

D,All,UX,0

D,All,UY,0

D,All,UZ,0

!Roller Support

NSEL,S,LOC,Z, 950/1000

NSEL,R,LOC,Y,-20/1000

D,All,UY,0

D,All,UX,0

! Symmetric boundary condition

NSEL,S,LOC,X, 60/1000

D,All,UX,0

! Loading

NSEL,S,LOC,Y, 160/1000

NSEL,R,LOC,Z, 450/1000

CM,A1,NODE

NSEL,S,LOC,Y, 160/1000

NSEL,R,LOC,Z, 450/1000

CM,A2,NODE

ALLSEL,ALL

CMGRP,A3,A1,A2

ALLSEL,ALL

CMSEL,S,A3

D,All,UY,-18/1000

!Run analysis

ANTYPE,0

NLGEOM,1

CNVTOL,F, ,0.1,2,0.01,

NSUBST,500,4000,50

OUTRES,ERASE

OUTRES,ALL,ALL

AUTOTS,1

LNSRCH,1

PRED,ON

NEQIT,200

TIME,1

ALLSEL

SOLVE

ANSYS APDL Code of EBRIG Strengthened RC beam with single layer of CFRP

(S2)

! units [MPa, N, mm]

FINISH

/CLEAR,,

/PREP7

!Volume block of concrete to be

Block,0,120/1000,15/1000,140/1000,0,1

!Divide the volume block at the location of discontinuity

/VIEW,1,1,1,1

/ANG,1

/REP,FAST

wpro,,-90,

wpoff,0,0,32/1000

VSBW, ALL

wpoff,0,0,84/1000

VSBW, ALL

wpro,,, 90

wpoff,0,0, 84/1000

VSBW, ALL

WPCSYS,-1,0

WPSTYLE,,,,,,,,,0 !

ASEL,S,LOC,Z,

AGEN,2,ALL, , , , 435/1000, ,0

ASEL,S,LOC,Z,

AGEN,2,ALL, , , , 465/1000, ,0

ASEL,S,LOC,Z,

AGEN,2,ALL, , , , 450/1000, ,0

ASEL,S,LOC,Z,

AGEN,2,ALL, , , , 550/1000, ,0

ASEL,S,LOC,Z,

AGEN,2,ALL, , , ,565/1000, ,0

ASEL,S,LOC,Z,

AGEN,2,ALL, , , ,535/1000, ,0

ASEL,S,LOC,Z,

AGEN,20,ALL, , , ,50/1000, ,0

ALLSEL,

VSBA,ALL,ALL

VSEL,S,LOC,Y,0,140/1000

CM,CONCRETEVOLUME1,VOLU

! definitions for concrete material property

fuc = 37.4E6 ! concrete cylinder strength

nu = 0.2

Ec = 28740E6

fut = 0.6*sqrt(fuc)

Oshear=0.2

Cshear=0.2

Cracking=fut

Crushing=-1

TCrackFactor=0.6

MPTEMP,,,,,,,,

MPTEMP,1,0

MP,EX,1,Ec

MP,NUXY,1,nu

TB,MISO,1,1,10,0

TBTEMP,0

TBPT,,0.000390397,11220000

TBPT,,0.000666928,17986437.45

TBPT,,0.000943459,23965750.59

TBPT,,0.00121999,28746196.96

TBPT,,0.001496521,32323156.41

TBPT,,0.001773051,34804621.01

TBPT,,0.002049582,36357604.4

TBPT,,0.002326113,37165280.46

TBPT,,0.002602644,37400000

TBPT,,0.0038,37400000

TB,CONC,1,1,9,


```
TYPE,1

MAT,1

CSYS,0

ESYS,0

! element sizing

CMSEL,S,CONCRETEVOLUME1

ASLV

LSLA

LESIZE,ALL,20/1000

VMESH,CONCRETEVOLUME1

!Part of Concrete volume block with fine meshing

Block,0,60/1000,0,15/1000,0,1

!Divide volume at the location of discontinuities

VSEL,S,LOC,Y,0,15/1000

wpoff,0,0,35/1000

VSBW, ALL

wpoff,0,0,15/1000

VSBW, ALL
```

wpoff,0,0,15/1000

VSBW, ALL

wpoff,0,0,10/1000

VSBW, ALL

wpoff,0,0,850/1000

VSBW, ALL

wpoff,0,0,10/1000

VSBW, ALL

wpoff,0,0,15/1000

VSBW, ALL

wpoff,0,0,15/1000

VSBW, ALL

WPCSYS,-1,0

WPSTYLE,,,,,,,,,0

wpro,,-90,

wpoff,0,0,10/1000

VSBW,ALL

wpro,,,90

wpoff,0,0,10/1000

VSBW,ALL

wpoff,0,0,24.5/1000

VSBW,ALL

wpoff,0,0,7/1000

VSBW,ALL

wpoff,0,0,15/1000

VSBW,ALL

WPCSYS,-1,0

WPSTYLE,,,,,,,,,0

!Select and delete part of block at the position of grooves

VSEL,S,LOC,X,34.5/1000,41.5/1000

VSEL,A,Loc,X,56.5/1000,60/1000

VSEL,R,LOC,Y,0,10/1000

VSEL,R,LOC,Z,75/1000,925/1000

VDELE,ALL, , ,1

VSEL,S,LOC,Y,0,15/1000

CM,CONCRETEVOLUME2,VOLU

!Define Element type for Concrete (for finer part of FE model)

ET,2,SOLID65

KEYOPT,2,1,1

KEYOPT,2,7,1

KEYOPT,2,8,1

TYPE,2

MAT,1

CSYS,0

ESYS,0

! meshing of lower part of concrete

CMSSEL,S,CONCRETEVOLUME2

ASLV

LSLA

LESIZE,ALL,5/1000

VMESH,CONCRETEVOLUME2

NSEL,S,LOC,Y,15

esln

ESEL,R,TYPE,,1

```
CM,Target\_1,ELEM

NSEL,S,LOC,Y,15

esln

ESEL,R,TYPE,,2

CM>Contact\_1,ELEM

Target1\_ETYPE=31

Contact1\_ETYPE=32

REAL,31

ET,Target1\_ETYPE,170

ET>Contact1\_ETYPE,174

KEYOPT>Contact1\_ETYPE,12,5

! Generate the target surface

!Generate Target surface

Type,Target1\_ETYPE

CMSEL,S,Target\_1

ESURF

! Generate the Contact Surface

TYPE>Contact1\_ETYPE
```

CMSEL,S,Contact_1

ESURF

!Creating blocks for steel plates

BLOCK,0,60/1000,140/1000,160/1000,435/1000,465/1000

BLOCK,0,60/1000,140/1000,160/1000,565/1000,535/1000

BLOCK,0,60/1000,0,-20/1000,35/1000,65/1000

BLOCK,0,60/1000,0,-20/1000,935/1000,965/1000

VSEL,S,LOC,Y,150/1000

wpoff,0,0, 450/1000

VSBW, ALL

wpoff,0,0, 100/1000

VSBW, ALL

wpro,,, 90/1000

wpoff,0,0, 19/1000

VSBW, ALL

!Make component of volumes of loading plates and element sizing

WPCSYS,-1,0

WPSTYLE,,,,,,,,,0

VSEL,S,LOC,Y,150

CM,LOADINGPLATE,VOLU

CMSEL,S,LOADINGPLATE,VOLU

ASLV

LSLA

LESIZE,ALL,20/1000

!Divide the volume of support plates at locations of discontinuities

VSEL,S,LOC,Y,-10

wpro,,90

wpoff,0,0,10/1000

VSBW,ALL

wpoff,0,0,24.5/1000

VSBW,ALL

wpoff,0,0,7/1000

VSBW,ALL

wpoff,0,0,15/1000

VSBW,ALL

WPCSYS,-1,0

WPSTYLE,,,,,,,,,0

! Make component of block of support plate and element sizing

VSEL,S,LOC,Y,-10

CM,SUPPORTPLATE,VOLU

CMSEL,S,SUPPORTPLATE,VOLU

ASLV

LSLA

LESIZE,ALL,5/1000

!Meshing of Steel plates

ET,3,185

TYPE, 3

MAT, 3

REAL, 3

ESYS, 0

SECNUM, ,

MSHAPE,0,3d

MSHKEY,1

CMSEL,S,LOADINGPLATE,VOLU

VMESH,LOADINGPLATE

CMSEL,S,SUPPORTPLATE,VOLU

VMESH,SUPPORTPLATE

!Merge the coincident nodes of concrete and loading plates

NSEL,S,LOC,Y,Beamheight

NSEL,A,LOC,Y,0

NUMMRG,NODE, , , ,LOW

!Create volume blocks of grooves (epoxy)

Block,34.5/1000,41.5/1000,0,10/1000,75/1000,925/1000

Block,56.5/1000,60/1000,0,10/1000,75/1000,925/1000

!Divide the volume block of epoxy at the locations of discontinuities

VSEL,S,LOC,X,34.5/1000,41.5/1000

VSEL,A,Loc,X,56.5/1000,60/1000

VSEL,R,LOC,Y,0,10/1000

VSEL,R,LOC,Z,75/1000,925/1000

wpro,,-90,

wpoff,0,0,4/1000

VSBW,ALL

wpoff,0,0,4/1000

VSBW,ALL

wpro,,,90

wpoff,0,0,35.5/1000

VSBW,ALL

wpoff,0,0,2.5/1000

VSBW,ALL

wpoff,0,0,2.5/1000

VSBW,ALL

wpoff,0,0,17/1000

VSBW,ALL

WPCSYS,-1,0

WPSTYLE,,,,,,,,,0

!Creating component of epoxy

VSEL,S,LOC,X,34.5/1000,41.5/1000

VSEL,A,Loc,X,56.5/1000,60/1000

VSEL,R,LOC,Y,0,10/1000

VSEL,R,LOC,Z,75/1000,925/1000

CM,EPOXYVOLUME,VOLU

!Material Modeling for Epoxy

MP,EX,6,5200E6

MP,NUXY,6,nu

TB,MISO,6,1,2,0

TBTEMP,0

TBPT,,0.0047,24.44E6

TBPT,,0.015,24.44E6

!Element sizing and meshing of epoxy elements

ET,6,SOLID185

!KEYOPT,6,2,3 ! simplified enhanced strain formulation

TYPE,6

MAT,6

R,6

REAL,6

CSYS,0

ESYS,0

CMSEL,S,EPOXYVOLUME

ASLV

LSLA

LESIZE,ALL,5/1000

VMESH,EPOXYVOLUME

!Generate area at the location of CFRP

ASEL,S,LOC,X,34.5/1000,35.5/1000

ASEL,A,LOC,X,40.5/1000,57.5/1000

ASEL,R,LOC,Y,0

ASEL,R,LOC,Z,75/1000,925/1000

AGEN,2,ALL,,,,,,0

ASEL,S,LOC,X,35.5/1000,40.5/1000

ASEL,A,LOC,X,57.5/1000,60/1000

ASEL,R,LOC,Y,8/1000

ASEL,R,LOC,Z,75/1000,925/1000

AGEN,2,ALL,,,,,,0

ASEL,S,LOC,X,35.5/1000

ASEL,A,LOC,X,40.5/1000

ASEL,A,LOC,X,57.5/1000

ASEL,R,LOC,Y,0,8/1000

ASEL,R,LOC,Z,75/1000,925/1000

AGEN,2,ALL,,,,,,,,0

ALLSEL

ASLV

ASEL,INVE

CM,CFRP,AREA

!Material model and section property of CFRP

MP,EX,5,230000*E6

MP,NUXY,5,nu

Local, 35,CART,0,0,0,0,0,-90

sect,5,shell,,EBRFRP

secdata, 0.12/1000,5,0.0,3

secdata, 0.12/1000,5,0.0,3

secoffset,MID

seccontrol,,,, , , ,

!Meshing of CFRP

CMSEL,S,CFRP

LSLA

LESIZE,ALL,5

ET,5,SHELL181

KEYOPT,5,1,1

R,5

TYPE,5

MAT, 5

REAL, 5

ESYS, 35

SECNUM,5

CMSEL,S,CFRP

CHKMSH,'AREA'

AMESH,CFRP

CSYS,0

!contact between concrete and CFRP at bottom

TB,CZM,99,,CBDD

TBDATA,1,,6.7*1000000,1.4/1000,1/1000,

!Contact between epoxy and concrete

TB,CZM,100,,CBDD

TBDATA,1,3.74*1000000,0.0005/1000,7.9*1000000,1.2/1000,1/1000,

!Contact 1

/COM, CONTACT PAIR CREATION - START

CM,_NODECM,NODE

CM,_ELEMCM,ELEM

CM,_KPCM,KP

CM,_LINECM,LINE

CM,_AREACM,AREA

CM,_VOLUCM,VOLU

/GSAV,cwz,gsav,,temp

MP,MU,100,

MAT,100

MP,EMIS,100,7.88860905221e-31

R,32

REAL,32

ET,33,170

ET,34,174

R,32,,,1.0,0.1,0,

RMORE,,,1.0E20,0.0,1.0,

RMORE,0.0,0,1.0,,1.0,0.5

RMORE,0,1.0,1.0,0.0,,1.0

RMORE,,,,,,1.0

KEYOPT,34,12,5

! Generate the target surface

ASEL,S,,760

CM,_TARGET,AREA

TYPE,33

NSLA,S,1

ESLN,S,0

ESLL,U

ESEL,U,ENAME,,188,189

NSLE,A,CT2

ESURF

CMSEL,S,_ELEMCM

! Generate the contact surface

ASEL,S,,981

ASEL,A,,1005

ASEL,A,,1026

CM,_CONTACT,AREA

TYPE,34

NSLA,S,1

ESLN,S,0

NSLE,A,CT2 ! CZMESH patch (fsk qt-40109 8/2008)

ESURF

ALLSEL

ESEL,ALL

ESEL,S,TYPE,,33

ESEL,A,TYPE,,34

ESEL,R,REAL,,32

/PSYMB,ESYS,1

/PNUM,TYPE,1

/NUM,1

```
EPlot

ESEL,ALL

ESEL,S,TYPE,,33

ESEL,A,TYPE,,34

ESEL,R,REAL,,32

CMSEL,A,\_NODECM

CMDEL,\_NODECM

CMSEL,A,\_ELEMCM

CMDEL,\_ELEMCM

CMSEL,S,\_KPCM

CMDEL,\_KPCM

CMSEL,S,\_LINECM

CMDEL,\_LINECM

CMSEL,S,\_AREACM

CMDEL,\_AREACM

CMSEL,S,\_VOLUCM

CMDEL,\_VOLUCM

/GRES,cwz,gsav
```

CMDEL,_TARGET

CMDEL,_CONTACT

/COM, CONTACT PAIR CREATION - END

!Similarly create contact elements at all contact surfaces

!*****

!Select lines at the location of longitudinal bars

LSEL,S,LOC,Y,BOTTOMCOVER

LSEL,R,LOC,X,SIDECOVER

CM,LON,LINE

CMSEL,S,LON

!Section property of rebar

SECTYPE,4,LINK, ,Rebar8mm

SECDATA,Mm8REBAR_AREA,

SECCONTROL,0,0

!Meshing of longitudinal rebar

ET,4,180

TYPE,4

MAT,2

SECNUM,4

TSHAP, LINE

LMESH,LON

!Select lines at the location of stirrups

LSEL,S,LOC,Y,74

LSEL,R,LOC,X,19/1000

LSEL,U,LOC,Z,0

LSEL,U,LOC,Z,435/1000

LSEL,U,LOC,Z,465/1000

LSEL,U,LOC,Z,535/1000

LSEL,U,LOC,Z,565/1000

LSEL,U,LOC,Z,1

CM,SV,LINE

LSEL,S,LOC,Y,32

LSEL,R,LOC,X,39.5/1000

LSEL,U,LOC,Z,0

LSEL,U,LOC,Z,435/1000

LSEL,U,LOC,Z,465/1000

LSEL,U,LOC,Z,535/1000

LSEL,U,LOC,Z,565/1000

LSEL,U,LOC,Z,1

CM,SB,LINE

LSEL,S,LOC,Y,116/1000

LSEL,R,LOC,X,39.5/1000

LSEL,U,LOC,Z,

LSEL,U,LOC,Z,435/1000

LSEL,U,LOC,Z,465/1000

LSEL,U,LOC,Z,535/1000

LSEL,U,LOC,Z,565/1000

LSEL,U,LOC,Z,1

CM,ST,LINE

CMGRP,Stirrups,SB,ST,SV

CMSEL,S,Stirrups

!Meshing of stirrups

TYPE, 4

MAT, 2

```
SECNUM,4

TSHAP, LINE

LMESH,Stirrups

/Solution

! Fixed boundary condition

NSEL,S,LOC,Y,-20/1000

NSEL,R,LOC,Z, 50/1000,

D,All,UX,0

D,All,UY,0

D,All,UZ,0

!Roller support

NSEL,S,LOC,Z, 950/1000

NSEL,R,LOC,Y,-20/1000

D,All,UY,0

D,All,UX,0

! Symmetric boundary condition

NSEL,S,LOC,X, 60/1000

D,All,UX,0
```

```
! Loading

!Select nodes at position of loading on steel plates

NSEL,S,LOC,Y, 140/1000

NSEL,R,LOC,Z, 450/1000

CM,A1,NODE

NSEL,S,LOC,Y, 140/1000

NSEL,R,LOC,Z, 550/1000

CM,A2,NODE

ALLSEL,ALL

CMGRP,A3,A1,A2

!Apply displacement on loading plate

ALLSEL,ALL

CMSEL,S,A3

D,All,UY,-15/1000

!Run analysis

ANTYPE,0

NLGEOM,1

CNVTOL,F, ,0.05,0.1,0.01,
```

NSUBST,500,4000,50

OUTRES,ERASE

OUTRES,ALL,ALL

AUTOTS,1

LNSRCH,1

PRED,ON

NEQIT,200

TIME,1

ALLSEL

SOLVE